Applied Geochemistry 159 (2023) 105815

Contents lists available at ScienceDirect

Applied Geochemistry

journal homepage: www.elsevier.com/locate/apgeochem

Adsorption of Ba and ^{226}Ra on illite: A comparative experimental and modelling study

Maria Marques Fernandes [a,*], Martina Klinkenberg [b], Bart Baeyens [a], Dirk Bosbach [b], Felix Brandt [b,**]

[a] Paul Scherrer Institut, Laboratory for Waste Management, 5232, Villigen, PSI, Switzerland
[b] Institute of Energy and Climate Research (IEK-6), Nuclear Waste Management, Forschungszentrum Jülich GmbH, 52425, Jülich, Germany

ARTICLE INFO

Editorial handling by Dr. Johannes Lützenkirchen

Keywords:
Radium
Barium
Illite
Adsorption
Modelling
Cation exchange
Selectivity
Competition

ABSTRACT

Illite, smectite and illite/smectite mixed layers are major phases in various argillaceous rock formations foreseen as potential host rocks for the deep geological disposal of high-level radioactive waste and are important sorbents for cationic radionuclides potentially released in the repository. ^{226}Ra is a critical radionuclide in the safety analysis and an important source of radioactivity in technically enhanced naturally occurring radioactive materials. A comprehensive study was carried out on the adsorption of Ba and Ra on purified homoionic Na-illite (Illite du Puy) over a wide range of experimental conditions (pH, concentration, ionic strength) allowing for the development of a quasi-mechanistic Ba/Ra adsorption model for illite. Ba adsorption isotherms obtained at fixed ionic strength and pH exhibit a non-linear behaviour in the Ba equilibrium concentration range between $\sim 10^{-7}$ and $\sim 10^{-2}$ M. The pH dependent adsorption of trace ^{226}Ra and Ba was investigated at different ionic strengths and evidenced a more pronounced adsorption of ^{226}Ra than Ba on illite. Finally, a competition experiment of trace ^{226}Ra in the presence of increasing Ba concentrations showed an unexpected ^{226}Ra adsorption behaviour which was not observed for montmorillonite in earlier studies. This large set of experimental data could be successfully modelled by Ba/^{226}Ra exchange reactions against Na, together with selectivity coefficients, on two different site types, namely planar sites and high affinity sites. The modelling of the pH dependent adsorption of Ba and ^{226}Ra at high ionic strength and high pH required an additional surface complexation reaction. Two additional exchange sites had to be introduced to quantitatively describe the ^{226}Ra uptake on illite in the ^{226}Ra/Ba competition experiment. The nature of these sites, however, remains unclear. The implementation of the ^{226}Ra adsorption model into predictive transport modelling codes is of key importance for the safety analysis of deep geological disposal of radioactive waste.

1. Introduction

Owing their low permeability and their high sorption capacity, clay minerals considerably retard the migration of potentially released cationic (radio-)contaminants in the geosphere and are therefore considered as geological (host rock) and engineered barriers (bentonite) in many deep geological radioactive waste repository concepts (Altmann, 2008) *e.g.* in Switzerland (Opalinus Clay (Nagra, 2002)), Belgium (Boom Clay (Ondraf, 2001)), France (Callovo-Oxfordian (Andra, 2001)), or Hungary (Boda Claystone (Károly and Zoltán, 2012)) and also commonly used for the remediation of contaminated environments (Wagner, 2013; Xu et al., 2017; Yuan et al., 2013; Zhu et al., 2016).

To account for these retardation properties in safety assessment studies, thermodynamic models capable of predicting the retention of radionuclides over a wide range of physico-chemical conditions are crucial. Important mechanisms that control the adsorption of cations on clay minerals are (i) cation exchange by electrostatic adsorption on the planar sites and (ii) surface complexation on the amphoteric edge sites. The former is dominating in the low to neutral pH range at low ionic strength for alkaline and alkaline-earth metals whereas the latter is mainly occurring at neutral to higher pH for strongly hydrolyzing metals (*e.g.*, Baeyens and Marques Fernandes, 2018).

Two clay minerals are of particular interest with respect to radionuclide migration in deep geological waste repositories, (i) illite as

* Corresponding author.
** Corresponding author.
E-mail addresses: maria.marques@psi.ch (M. Marques Fernandes), f.brandt@fz-juelich.de (F. Brandt).

https://doi.org/10.1016/j.apgeochem.2023.105815
Received 2 May 2023; Received in revised form 8 August 2023; Accepted 17 October 2023
Available online 19 October 2023

common mineral and main component of several argillaceous formations, and (ii) montmorillonite as main component of bentonites used as technical barrier (Andra, 2001; Missana et al., 2017; Nagra, 2014). While both clay minerals are well studied with respect to their adsorptive retention capabilities for divalent metals such as *e.g.*, Zn, Sr, Co and Pb (Marques Fernandes and Baeyens, 2019; Montoya et al., 2018), little experimental data is so far available on the retention of Ra.

Ra is a decay product of ^{232}Th, ^{235}U and ^{238}U. ^{226}Ra, the isotope of major concern, is safety relevant due to its high radiological risk (long-lived alpha emitters $t_{1/2}$ = 1600 y) and must be treated or disposed accordingly. Worldwide its sources are multiple from natural, past legacies to nowadays technologically enhanced. ^{226}Ra is ubiquitous in radioactive waste originating from *e.g.*, nuclear industry (in spent nuclear fuel or other wastes from processing uranium ore), former industry (radioluminescent devices, contaminated slag, incinerator waste) and medicine (sealed and unsealed sources for cancer therapy). The fate of ^{226}Ra in the environment is also relevant because it is an important source of radioactivity in **t**echnically **e**nhanced **n**aturally **o**ccurring **r**adioactive **m**aterials (TENORM) (Alhajji et al., 2016; IAEA, 2014). NORM containing ^{226}Ra originates essentially from mining (*e.g.*, uranium, phosphate and even gold) and milling operations, from coal ash, and raw material production processes *e.g.*, oil extraction, geothermal energy production (Fisher, 1998; Martin et al., 2003).

Ames et al. (1983) quantified the adsorption of ^{226}Ra on clinoptilolite, montmorillonite, nontronite, opal, silica gel, illite and kaolinite, and described it by an empirical Freundlich equation. They postulated that the adsorption of ^{226}Ra increases as a function of cation exchange capacity, with the exception of montmorillonite suggesting that other processes might control ^{226}Ra uptake. Hidaka et al. (2007) concluded from observations at the Oklo uranium deposit that illite played a key role in the fixation or retardation of radioisotopes with selective adsorption of ^{226}Ra.

Only a few studies have systematically addressed the adsorption of ^{226}Ra or Ba (as its potential chemical analogue) on clay minerals *e.g.,* as a function of pH (pH-edge) or ^{226}Ra/Ba-concentration (isotherm) or by spectroscopic techniques. Tachi et al. (2001) quantified the adsorption of ^{226}Ra onto bentonite and purified montmorillonite as a function of pH, ionic strength and liquid to solid ratio by batch experiments. On montmorillonite, the data was modelled by assuming cation exchange on the planar sites and surface complexation at edge sites at higher pH values. On bentonite, ^{226}Ra adsorption could be reproduced by assuming only cation exchange. The formation of inner sphere complexes at high pH was confirmed at least for Ba onto montmorillonite by applying X-ray Absorption Spectroscopy in the study of Zhang et al. (2001). Robin et al. (2017) investigated the adsorption of ^{226}Ra on beidellite, a smectite with tetrahedral charge, as a function of pH. To model their data, a multi-site ion-exchange model was applied. Klinkenberg et al. (2021) confirmed the observation of Tachi et al. (2001) for ^{226}Ra adsorption on montmorillonite. Klinkenberg et al. (2021) performed additionally similar experiments with Ba and observed a close but not always an identical adsorption behaviour for both elements. According to these authors, Ba can be viewed as a good analogue for ^{226}Ra regarding the adsorption on montmorillonite at ionic strengths < 0.1 M and pH < 8 but not for adsorption at higher ionic strength.

For illite or illite rich samples, however, ^{226}Ra adsorption data is much sparser. Alhajji et al. (2016) found distribution factors (K_d) for ^{226}Ra adsorption to be low for bentonite, and relatively high for illite. Missana et al. (2017) carried out ^{226}Ra and Ba adsorption experiments on clay rich samples (illite content ranging from 35 to 65% and illite-smectite mixed layers from 25 to 70%, respectively) from the French Gault and Plicatules formations in different forms (Na, NH_4, Ca). They observed a much stronger adsorption of ^{226}Ra compared to Ba onto their argillaceous samples and modelled the Ba and Ra data by considering cation exchange and at higher pH surface complexation. At high ionic strength, the authors had to include high energy sites (HES) to describe their experimental data on Na- and NH_4-exchanged clays.

This study presents detailed and systematic experimental and modelling investigations to improve the quantitative understanding of Ba and ^{226}Ra adsorption on illite as well as the applicability of Ba as a chemical analogue for ^{226}Ra with respect to the adsorption on illite. The adsorption of Ba and Ra was studied in a large number of single element experiments as a function of pH and ionic strength. Furthermore, in an additional experiment the adsorption of trace ^{226}Ra was quantified as a function of increasing Ba concentrations, to investigate the competitive adsorption behaviour of both elements and to better constrain the adsorption model for Ba and Ra on illite.

2. Materials and methods

2.1. Preparation and conditioning of illite

The preparation and conditioning of the illite (Na-illite, IdP-2; Illite de Puy, Le Puy-en-Velay, France) suspensions was carried out following the methodology described in Bradbury and Baeyens (2009). The procedure consists of several washing steps in 1 M NaCl, purifying the clay from soluble salts and converting it into a homoionic Na-form (Na-IdP). The grain size fraction < 0.5 μm was obtained from a flocculation/peptization procedure, separated and treated with acid before adjusting the desired background electrolyte (NaCl) concentration by dialysis techniques as well as the solid liquid ratio (S/L).

The cation exchange capacity (CEC) of the purified IdP suspensions was measured by the ^{134}Cs isotopic dilution method (Baeyens and Bradbury, 2004). A large number of CEC determinations on different illite batches carried out at neutral pH yielded average values of 225 ± 10 meq·kg^{-1} (Marques Fernandes and Baeyens, 2019).

2.2. Batch adsorption experiments

Batch adsorption experiments were carried out following the protocol described in Klinkenberg et al. (2021) and in Marques Fernandes and Baeyens (2019). Adsorption of Ba was determined at various fixed ionic strengths as a function of pH at trace ^{133}Ba concentrations (pH-edges) and at constant pH and ionic strength as function of increasing Ba concentrations (isotherms). ^{226}Ra adsorption was only measured at trace Ra concentrations as a function of pH and ionic strength since high ^{226}Ra amounts are difficult to handle due to radiological safety concerns. Instead, the competitive adsorption behaviour of Ba vs. Ra was investigated by measuring the adsorption of trace ^{226}Ra as a function of increasing ^{137}Ba (*i.e.,* along the Ba isotherm). Assuming Ba and ^{226}Ra were true chemical analogues, this should result through isotopic dilution in a similar adsorption of Ba and Ra (*i.e.,* Ra following the Ba isotherm).

All experiments were carried out at 21 ± 2 °C and under air atmosphere at defined S/L (see Table 1). A pH drift was prevented by adding the buffers $C_6H_{13}NO_4S$ (MES) pKa = 6.15, $C_7H_{15}NO_4S$ (MOPS) pKa = 7.2, $H_2NC(CH_2OH)_3$ (TRIS), pKa = 8.06, or $C_8H_{17}NOS$ (CHES), pKa = 9.55 in concentrations of 2 mM. These buffers were chosen because of their weak complexation behaviour towards earth-alkaline metals at the used concentration (Ferreira et al., 2015; Perrin, 1974). The pH was adjusted with 1 M NaOH and 1 M HNO_3 without affecting the ionic strength. For each experimental series, the S/L was measured by drying to constant weight at 105 °C and correcting for the salt content. All solutions were prepared from ultrapure deionized water (18.2 MΩ·cm^{-1} at 25 °C) and analytical grade chemicals. Well characterized stock solutions of ^{133}Ba ($t_{1/2}$ = 10.55 a; Eckert & Ziegler Isotope Products Laboratories, California, USA) and ^{226}Ra ($t_{1/2}$ = 1200 a, prepared from $RaBr_2$) were used. The radiotracers were diluted from the stock solutions in the respective background electrolyte and equilibrated overnight. For the experiments, the tracer solutions were adjusted in pH by adding the buffer. In a third step, the clay suspension was added, starting the adsorption. All experiments were carried out as duplicates in 50 mL polyethylene centrifuge tubes, which were mounted into end-over-end

Table 1
Summary of the Ba and ^{226}Ra adsorption experiments on Na-IdP.

Element	Type of experiment	[Ba_{init} or Ra_{init}] (M)	[Ba_{eql}] (M)	NaCl (M)	S/L (g· L^{-1})	pH
^{133}Ba/^{137}Ba	Isotherm	–	$2.2{\cdot}10^{-10}$ – $7.2{\cdot}10^{-3}$	0.02	2.0 – 9.6	5.1
^{133}Ba/^{137}Ba	Isotherm	–	$1.8{\cdot}10^{-9}$ – $1.9{\cdot}10^{-2}$	0.02	1.3	6.6
^{133}Ba/^{137}Ba	Isotherm	–	$2.6{\cdot}10^{-10}$ – $1.0{\cdot}10^{-2}$	0.02	1.1 – 11.2	6.9
^{133}Ba/^{137}Ba	Isotherm	–	$1.2{\cdot}10^{-10}$ – $6.9{\cdot}10^{-3}$	0.02	2.0 – 9.6	7.6
^{133}Ba/^{137}Ba	Isotherm	–	$3.7{\cdot}10^{-11}$ – $7.2{\cdot}10^{-3}$	0.02	3.6 – 17.3	9.0
^{133}Ba	Edge	$7.7{\cdot}10^{-8}$	–	0.02	1.3	5.1– 10.9
^{133}Ba	Edge	$3.6{\cdot}10^{-8}$	–	0.03	2.2	5.3 – 9.3
^{133}Ba	Edge	$3.6{\cdot}10^{-8}$	–	0.3	1.9	5.5–10.6
^{226}Ra	Edge	$8.0{\cdot}10^{-8}$	–	0.02	1.3	5.5 – 11.5
^{226}Ra	Edge	$1.9{\cdot}10^{-8}$	–	0.14	15.1	5.5 – 9.3
^{226}Ra	Edge	$1.9{\cdot}10^{-8}$	–	0.3	5.8	5.6 – 9.4
^{226}Ra/^{137}Ba	Isotherm[a]	$1.4{\cdot}10^{-7}$ (^{226}Ra)	$3.5{\cdot}10^{-8}$ – $1.8{\cdot}10^{-2}$	0.02	1.3	7.0

[a] Ba isotherm in the presence of trace ^{226}Ra.

shakers to react for 7 days. Kinetic experiments were carried out to ensure that 7 days were sufficient for equilibration (Marques Fernandes et al., 2023) as well as blank experiments to check for potential wall adsorption of the radiotracers.

The adsorption was quantified by measuring the activity or the concentration of the given cation in the supernatant. The phase separation in the Ba-experiments was performed by centrifuging with a Beckman Coulter Avanti™ J30i High-Performance centrifuge (1 h at 108 000 *g* max.) whereas a Heraeus Multifuge SR3+ (Thermo Scientific; 1 h at 3000 g at 20 °C) was used for the ^{226}Ra experiments. For the ^{226}Ra experiments at low ionic strength, the supernatant solution was filtered through Advantec ultrafilters (MWCO = 10 000 Da) to avoid colloids. The combination of centrifugation and ultrafilatration results in a similar cut-off size as the ultracentrifugation. Earlier studies by Curti et al. (2010) demonstrated that ^{226}Ra does not adsorb onto these filters. The pH of each sample was measured using a Metrohm combined electrode. A summary of all the experiments carried out together with the main experimental conditions is given in Table 1.

2.2.1. Adsorption isotherms

The adsorption isotherms were carried out with stable Ba solutions labelled with ^{133}Ba, in 0.02 M NaCl (Table 1, details are provided in Marques Fernandes et al. (2023)) at pH 5.1, 6.6, 6.9, 7.6 and 9.0. Each standard solution containing ^{133}Ba was equilibrated at least overnight before use to account for potential tracer wall adsorption. In the same way, stable Ba solutions were labelled with trace ^{226}Ra to follow the adsorption of Ra. The experimental conditions employed for this experiment are very similar to the Ba isotherms measured in 0.02 M NaCl at pH ~7 (see Table 1).

2.2.2. pH dependent adsorption

Adsorption edges of Ba were determined in the pH range 5 – 11. ^{133}Ba solutions with concentration between $3.6{\cdot}10^{-8}$ and $7.7{\cdot}10^{-8}$ M were equilibrated with Na-IdP at ionic strengths of 0.02 – 0.3 M NaCl (Table 1, details provided in Marques Fernandes et al. (2023)). For ^{226}Ra, adsorption edges were collected within the pH range 5 – 12 at ionic strengths between 0.02 and 0.3 M NaCl, following the same procedure as for Ba.

2.3. Analytical methods

A Canberra Packard Cobra Quantum gamma counter was utilized for the determination of the ^{133}Ba activity of aliquots of the supernatants. Labelled standard solutions were prepared at the start of the adsorption experiments and measured simultaneously. The concentration of ^{226}Ra was quantified with the ultra-low-level liquid scintillation (LSC) counter Qantulus (PerkinElmer, USA). Samples for the LSC were prepared by mixing 19 mL of Ultima Gold LLT cocktail with 1 mL aliquots of the supernatants. Gluing the LSC glass vials gas tight prevented the release of Rn, so that measurements of the samples could be carried out in equilibrium condition of ^{226}Ra and Rn after 38 days. An ICP-MS ELAN 6100 DRC (PerkinElmer SCIEX) was used for analyses of stable ^{137}Ba in the combined Ba/^{226}Ra experiments. Before the analysis, the samples were diluted and acidified with HNO_3.

2.4. Adsorption modelling

Ra^{2+}-Na^{+} and Ba^{2+}-Na^{+} exchange reactions on cation exchange sites, mainly controls the adsorption of Ra and Ba on Na-IdP. Generally, the cation exchange reaction can be written as follows:

$$2\ \text{Na-}^{X}\text{IdP} + \text{Me}^{2+} \Leftrightarrow \text{Me-}^{X}\text{IdP} + 2\ \text{Na}^{+} \quad (1)$$

with x representing the cation exchange site and Me^{2+} being Ra^{2+} or Ba^{2+}. To quantify the reaction in terms of a so-called selectivity coefficient a mass action law is normally used. The numerical values of the selectivity coefficients derived from experimental data depend on the thermodynamic model used for the interpretation measurements. According to the Gaines and Thomas convention (Gaines and Thomas, 1953), the fractional scale for the adsorbed cations and the molarity scale for the cations in solution have been used, and the selectivity coefficient (K_c) is defined as:

$$K_{c_{Na}}^{Me} = \frac{N_{Me}}{N_{Na}^{2}} \frac{\left[Na_{eql}\right]^{2}}{\left[Me_{eql}\right]} \frac{(\gamma_{Na})^{2}}{\gamma_{Me}} \quad (2)$$

where N_{Me} and N_{Na} are the equivalent fractional occupancies of Me (*i.e.,* Ra or Ba) and Na, respectively, defined as the equivalent of Me or Na adsorbed per kg of clay mineral divided by the cation exchange capacity of the exchange site (CEC_X) [eq·kg^{-1}]. [Na_{eql}] and [Me_{eql}] are aqueous equilibrium concentrations (M) of Me and Na and γ_{Na} and γ_{Me} aqueous phase activity coefficients.

By fitting the experimental data with the aforementioned cation exchange reaction on the different cation exchange sites, the ${}^{Me}_{Na}K_c$ values on the cation exchange sites of illite were derived. It will be shown that two and four different cation exchange sites were required for Ba and Ra, respectively, to quantitatively describe the adsorption behaviour onto illite for the 12 experimental data sets presented in this study (see Table 1).

To model the Ba and Ra edges at pH > 8, an additional adsorption mechanism had to be considered. In this region, the 2 site protolysis non-electrostatic surface complexation (2SPNE SC/CE) model for illite (Bradbury and Baeyens, 2009) was applied. The uptake of Ra/Ba was described by surface complexation on the amphoteric edge sites of the illite platelets. The site types, capacity and protolysis constants of these adsorption sites are defined in the 2SPNE SC/CE model. The surface complexation constants for ^{226}Ra and Ba derived in this study were obtained by fitting the experimental data.

All the thermodynamic calculations presented in this study were performed with the code MINSORB (Bradbury and Baeyens, 1997),

which was derived from geochemical code MINEQL (Westall et al., 1976) and which contains subroutines for calculating cation exchange and surface complexation reactions simultaneously. Aqueous activity coefficients were calculated using the Davies equation (Davies, 1962) with a value of 0.3 for the C_D constant.

3. Results and modelling

In order to avoid unnecessary repetition, the experimental results of the ^{226}Ra and Ba adsorption data are presented and discussed together with the modelling. The adsorption isotherms at different pH and edges at different ionic strength obtained for Ba onto illite are presented in section 3.1. Ra edge data at different ionic strengths are treated in a section 3.2. Note that due to radiological restrictions, ^{226}Ra isotherms could not be determined experimentally. Finally, section 3.3 addresses the experimental and modelling results of a competitive experiment of trace ^{226}Ra adsorption in the presence of increasing ^{137}Ba concentrations.

The adsorption of Ba or Ra (Me) is usually quantified by the solid-liquid distribution ratio R_d ($L{\cdot}kg^{-1}$), which is defined as:

$$R_d = \frac{[Me_{ads}]}{[Me_{eql}]} \quad (3)$$

where $[Me_{ads}]$ are the moles of Me (*i.e.*, Ba or Ra) adsorbed per kg of clay mineral and $[Me_{eql}]$ the aqueous equilibrium concentrations (M). If the adsorption mechanism is cation exchange the amount of Me adsorbed in $mol{\cdot}kg^{-1}$ on site x can be expressed from Eq. (2) as $[Me_{ads}] = \frac{N_{Me}\cdot CEC_x}{2}$, allowing Eq. (3) to be re-written as:

$$R_d = N_{Me}\cdot\frac{CEC_x}{2}\cdot\frac{1}{[Me_{eql}]} \quad (4)$$

At trace Me concentration, N_{Na} can be taken ~1 and R_d can be re-written by combining Eq. 2 and Eq. 4 to yield an expression relating the selectivity coefficient (K_c) to the adsorption (R_d), *i.e.*

$$R_d = {}^{Me}_{Na}K_c\cdot\frac{1}{2}\cdot CEC_x\cdot\frac{\gamma_{Me}}{\gamma^2_{Na}}\cdot\frac{1}{[Na]^2} \quad (5)$$

where all the parameters are defined previously.

Ba and Ra adsorption edges are plotted as log R_d *vs* pH. The Ba isotherms are plotted either as log R_d *vs* log $[Ba_{eql}]$ or as the log $[Ba_{ads}]$ *vs* log $[Ba_{eql}]$. The Ba/Ra competition results are presented as log R_d Ba/^{226}Ra *vs* log $[Ba_{eql}]$.

The experimental and modelling results are provided in Tables A1 to A16 of the appendix and further information in the data publication (Marques Fernandes et al., 2023).

3.1. Adsorption of Ba on Na-IdP: experimental and modelling

3.1.1. Ba isotherms in 0.02 M NaCl

Five Ba adsorption isotherms on Na-IdP in 0.02 M NaCl at pH = 5.1, 6.6, 6.9, 7.6 and 9.0 were determined using ^{133}Ba as isotopic tracer to monitor stable ^{137}Ba concentrations in the liquid phase after equilibrium. One Ba adsorption isotherm in the presence of trace ^{226}Ra at pH 7.0 was carried out with ^{137}Ba only. The experimental conditions are summarized in Table 1 and the results (symbols) are shown in Fig. 1.

As illustrated in Fig. 1, all isotherms quantitatively showed the same adsorption behaviour across the entire Ba concentration range, and clearly, no pH dependency between pH 5 and 9 was observed. Furthermore, the agreement between two independent analytical methods is illustrated in the isotherm at pH 7.0. The experimental data determined by ICP-MS for this isotherm, however, scatter more at high $[Ba_{eql}]$.

All five isotherms exhibited an overall non-linear behaviour (see Fig. 1b). At low $[Ba_{eql}]$ the adsorption is linear (Langmuir type, slope equal 1), whereas with increasing Ba concentration the adsorption becomes non-linear. The non-linearity of the isotherms at $3{\cdot}10^{-8}$ M < $[Ba_{eql}]$ < $3{\cdot}10^{-5}$ M suggests adsorption on at least two different sites. High Ba adsorption was observed at $[Ba_{eql}] < 10^{-7}$ M (log R_d = 4 – 4.4 $L{\cdot}kg^{-1}$) which decreased steadily as function of increasing $[Ba_{eql}]$ and reached very low Ba adsorption at $[Ba_{eql}]$ ~10^{-2} M (log R_d ~ 1 $L{\cdot}kg^{-1}$). The cation exchange reaction given by Eq. (1) and taking a CEC of 225 meq•kg^{-1} representing the planar sites (PS) of illite was considered in a first step in the fitting of the Ba data. The only adjustable parameter used was $^{PS}K_c$ (Ba–Na). The experimental adsorption data for Ba in the concentration range $3{\cdot}10^{-6}$ M to 10^{-2} M are best reproduced with log $^{PS}K_c$ (Ba–Na) = 1.05 as illustrated by the dashed-dotted lines (model PS) in Fig. 1. Clearly, the model PS curve representing cation exchange on the PS underestimates the experimental Ba R_d values at $[Ba_{eql}] < 3{\cdot}10^{-6}$ M by 0.8 log units. A second cation exchange site denoted as high affinity site (HAS) was introduced to fit the Ba adsorption at low concentration. The same type of cation exchange reaction as given in Eq. (1) and associated selectivity coefficient given in Eq. (2) was used where both, the site capacity of the HAS and the K_c value are adjustable parameters. The best fit of the experimental R_d data for Ba in the concentration range 10^{-10} M < $[Ba_{eql}]$ < $3{\cdot}10^{-6}$ M on HAS using a site capacity of 5 $meq{\cdot}kg^{-1}$ for HAS and log $^{HAS}K_c$ (Ba–Na) of 3.4 is illustrated by the dotted lines. The fit of the overall adsorbed Ba on the PS and the HAS are shown in Fig. 1 by the black solid line and represented the best fit to the Ba isotherms measured in 0.02 M NaCl in the pH range from 5 to 9. Fig. 1b illustrates the saturation of HAS and PS sites by the dotted and dashed-dotted lines, respectively. At the highest $[Ba_{eql}]$ concentration the PS are saturated with Ba and are in good agreement with the CEC of 225 $meq{\cdot}kg^{-1}$ for Na-IdP.

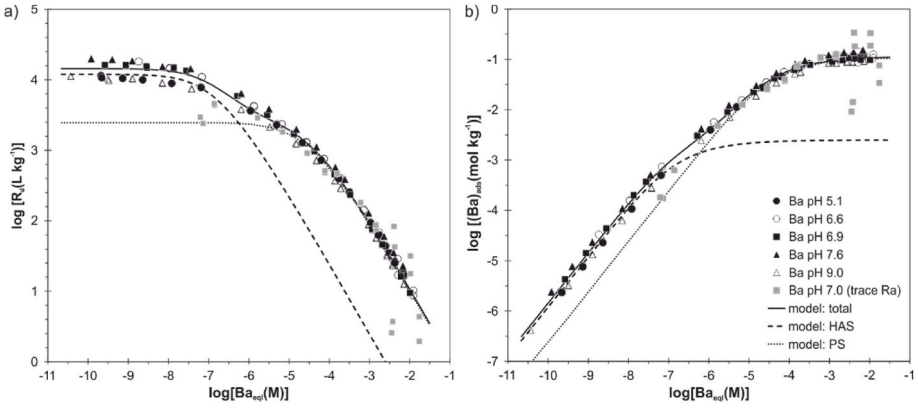

Fig. 1. Adsorption isotherms of ^{133}Ba/^{137}Ba on Na-IdP in 0.02 M NaCl at pH 5.1, 6.6, 6.9, 7.6 and 9.0. Grey symbols represent the ^{226}Ra/^{137}Ba isotherm on Na-IdP in 0.02 M NaCl at pH 7.0 (see text for details).

3.1.2. Ba edges in 0.02 M, 0.03M and 0.3 M NaCl at pH 5 to 11

The experimental Ba adsorption edges on Na-IdP in 0.02 M, 0.03 M and 0.3 M NaCl and the corresponding modelling are shown in Fig. 2. The Ba adsorption edges show no pH dependency up to pH 8 and decreases as a function of increasing ionic strength. The decrease of adsorption with increasing ionic strength is typical for cation exchange due to competitive effects of the background cation, see Eq. (2) (*e.g.,* Tertre et al. (2011); Klinkenberg et al. (2021)). At high pH, there is a trend of increasing Ba adsorption that is most pronounced at high ionic strength (Fig. 2c). Ba adsorption on Na-montmorillonite showed a very similar behaviour (Klinkenberg et al., 2021).

Ba adsorption at trace concentration is dominated by cation exchange on HAS as shown in Fig. 1 In the fitting procedure, the site capacities of HAS and PS as well as $^{PS}K_c$ (Ba–Na), derived in section 3.1.1, were fixed. The contribution of the adsorption of Ba on the PS is illustrated in Fig. 2 by the dashed lines. Clearly, Ba adsorption on PS is small as expected from the isotherm modelling. The pH independent part of the edges was reproduced by the best fit value for $^{HAS}K_c$ (Ba–Na). The result of this fitting procedure is illustrated in Fig. 2 by the dotted lines. As can be seen from the total calculated adsorption (solid lines) up to pH 8 Ba adsorption is well described by cation exchange. The results in Table 3 show that the $^{HAS}K_c$ (Ba–Na) values increase at increasing ionic strength. This trend was also observed for Ba–Na exchange on the PS of montmorillonite (Klinkenberg et al., 2021).

The contribution of surface complexation to the adsorption of Ba shown by the broken dotted lines in Fig. 2 was calculated with the 2SPNE SC/CE model developed for illite (Bradbury and Baeyens, 2009). In this model, 2 different amphoteric type sites are considered. The pK_a values of the weak type 1 sites ($\equiv S^{W1}OH$) and weak type 2 sites ($\equiv S^{W2}OH$) are 6.5 and 9.5, respectively. Strongly hydrolyzing metals such as divalent transition and trivalent lanthanides form surface complexes on $\equiv S^{W1}OH$ sites whereas weakly hydrolyzing metals form surface complexes on $\equiv S^{W2}OH$ sites. In the present modelling, the adsorption of Ba was calculated assuming one surface complexation

Table 2
Capacity of the cation exchange (PS and HAS) and surface complexation sites ($\equiv S^{W2}OH$). Protolysis reactions and constants for the $\equiv S^{W2}OH$ sites.

Site type	Capacity
HAS	$5{\cdot}10^{-3}$ eq·kg^{-1}
PS	0.225 eq·kg^{-1}
$\equiv S^{W2}OH$	$40{\cdot}10^{-3}$ mol·kg^{-1}
Protolysis reaction	**log K**
$\equiv S^{W2}OH + H^+ \Rightarrow \equiv S^{W2}OH_2^+$	8.5
$\equiv S^{W2}OH \Rightarrow \equiv S^{W2}O^- + H^+$	−10.5

Table 3
Summary of the selectivity coefficients (K_c) for Ba^{2+}-Na^+ exchange on PS and HAS and Ba SC constant on weak sites ($\equiv S^{W2}OH$) of Na-IdP.

Experiment	Isotherm	Edges		
NaCl background concentration (M)	0.02	0.02	0.03	0.3
pH	5.1 – 9.0	5 – 11		
Cation exchange reactions	log K_c (Ba–Na)			
$2Na\text{-}PS + Ba^{2+} \Leftrightarrow Ba\text{-}PS + 2Na^+$	1.05	1.05	1.05	1.05
$2Na\text{-}HAS + Ba^{2+} \Leftrightarrow Ba\text{-}HAS + 2Na^+$	3.4	3.4	3.7	4.3
SC reaction on weak 2 sites	**log ^{W2}K**			
$\equiv^{W2}SOH + Ba^{2+} \Leftrightarrow \equiv^{W2}SOBa^+ + H^+$	−4.2			

reaction on $\equiv S^{W2}OH$ given by

$$\equiv S^{W2}OH + Ba^{2+} \Leftrightarrow \equiv S^{W2}OBa^+ + H^+$$

with a SC constant log $^{W2}K = -4.6$. The non-adjustable parameters (site capacity and protolysis constants for the $\equiv S^{W2}OH$ sites) are summarized in Table 2. These parameters are fixed for the fitting of the selectivity constants provided in Tables 3 and 4.

At low ionic strength, the adsorption of Ba is dominated by cation exchange and the contribution of surface complexation of Ba on the edge sites is small as shown by the broken dotted lines in Fig. 2a and b. In the case of high ionic strength where cation exchange is suppressed by

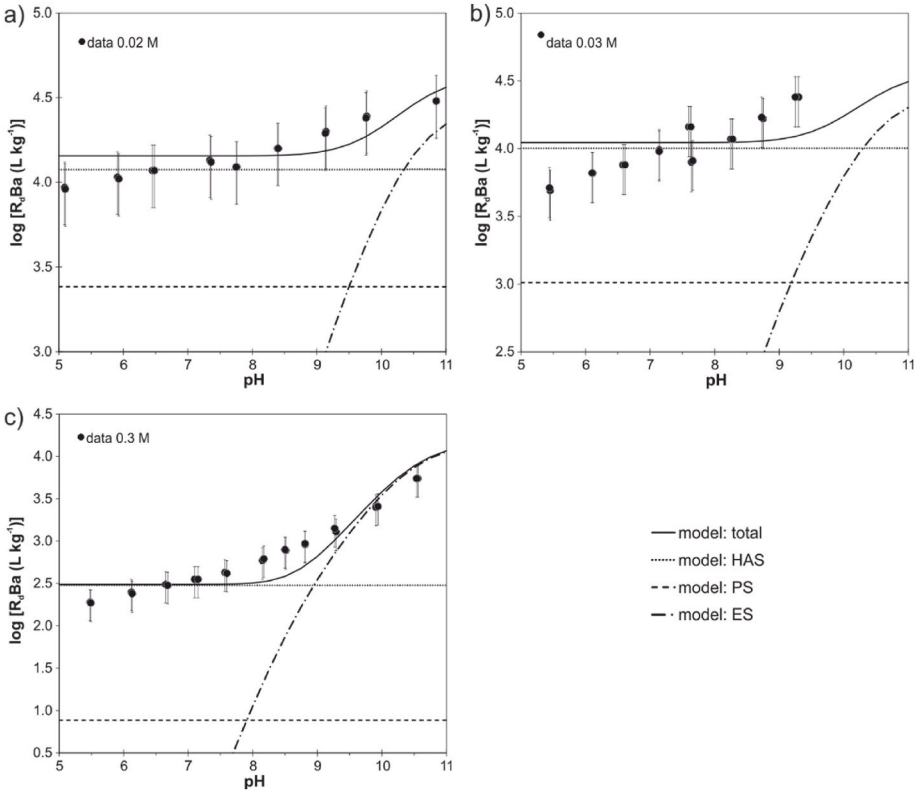

Fig. 2. Adsorption edges of Ba on Na-IdP in (a) 0.02 M NaCl, (b) 0.03 M NaCl and (c) 0.3 M NaCl. Experimental and modelling.

Table 4
Summary of the selectivity coefficients (K_c) for Ra^{2+}-Na^+ exchange on PS and HAS and Ra SC constant on weak sites ($\equiv S^{W2}OH$) of Na-IdP.

Experiment	Edges		
NaCl background concentration (M)	0.02	0.13	0.3
pH	5 – 11		
Cation exchange reactions	**log K_c (Ra–Na)**		
2Na-PS + Ra^{2+} ⇔ Ra-PS + $2Na^+$	1.05	1.05	1.05
2Na-HAS + Ra^{2+} ⇔ Ra-HAS + $2Na^+$	4.1	4.2	4.7
SC reaction on weak 2 sites	**log ^{W2}K**		
$\equiv^{W2}SOH + Ra^{2+} \Leftrightarrow \equiv^{W2}SORa^+ + H^+$	3.4		

competition of the counter cation Na, the contribution of surface complexation to the overall adsorption is more pronounced (Fig. 2c). The thermodynamic constants used for the cation exchange and surface complexation modelling of Ba on Na-IdP obtained from the isotherms (section 3.1.1) and the pH edges (section 3.1.2) are summarized in Table 2.

3.2. Adsorption edges of Ra on Na-IdP: experimental and modelling

The ^{226}Ra adsorption edges on Na-IdP determined in 0.02 M, 0.14 M and 0.3 M NaCl are illustrated in Fig. 3 and Tables A10-12. The adsorption behaviour of Ra is very reminiscent to Ba and the 3 edges show no pH dependency up to pH ~8 whereas adsorption decreases at increasing ionic strength. However, Ra shows a more pronounced adsorption than Ba at the same ionic strength (see Fig. 2a and c and Fig. 3a and c). Ames et al. (1983) carried out batch experiments (S/L = 50 g·L^{-1}, 25 °C, I = 0.01 M NaCl, pH = 7) on a Na-illite of a different origin with a CEC = 250 meq·kg^{-1}. Already these authors expected a much lower Ra-adsorption for illite compared to montmorillonite at identical experimental conditions, based on the much lower CEC of illite. A lower R_d was calculated using the data of Ames et al. (1983) for montmorillonite in comparison to their illite data, confirming the observations of Klinkenberg et al. (2021).

Fig. 3 shows that the adsorption of Ra increases at pH > 8 as was observed by Tachi et al. (2001) and Klinkenberg et al. (2021) for montmorillonite. This is due to Ra adsorption on the amphoteric edge sites of illite.

In a similar way as for Ba, the Ra adsorption edges were modelled using the 2SPNE SC/CE model. The site types and capacities derived from the Ba adsorption data given in Table 2 were used for the modelling of the Ra edges. Only trace Ra adsorption could be fitted since no Ra isotherm data are available. The cation exchange behaviour of Ra on the planar sites is assumed to be similar as for Ba and is low. The adsorption of Ra on the HAS is dominating the total uptake of Ra on Na-IdP. The modelling parameters to fit the experimental data are summarized in Table 4 and are shown in Fig. 3. Similar as for Ba–Na exchange on HAS, the selectivity coefficients for Ra–Na exchange increase at increasing ionic strength.

The surface complexation contribution to the adsorption of Ra indicated by the broken dotted lines in Fig. 3 was calculated by considering one surface complexation reaction on the weak type 2 sites given by $\equiv S^{W2}OH + Ra^{2+} \Leftrightarrow \equiv S^{W2}ORa^+ + H^+$ with a SC constant log $^{SC}K = -3.4$.

Table 4 summarizes the cation exchange and surface complexation reactions together with the selectivity coefficients and surface complexation constant for Ra adsorption on Na-IdP. In contrast to Ba (Table 3) the adsorption of Ra on HAS is more pronounced and the surface complexation of Ra on $\equiv S^{W2}OH$ sites is stronger which is reflected by the higher selectivity coefficients and the stronger surface complexation constant. On montmorillonite Ba and Ra adsorption behaviour was similar (Klinkenberg et al., 2021), whereas the adsorption behaviour of Ba/Ra on HAS and $\equiv S^{W2}OH$ sites of illite is different and hence Ba and Ra cannot be considered as chemical analogues. Note that HAS sites were not observed on montmorillonite.

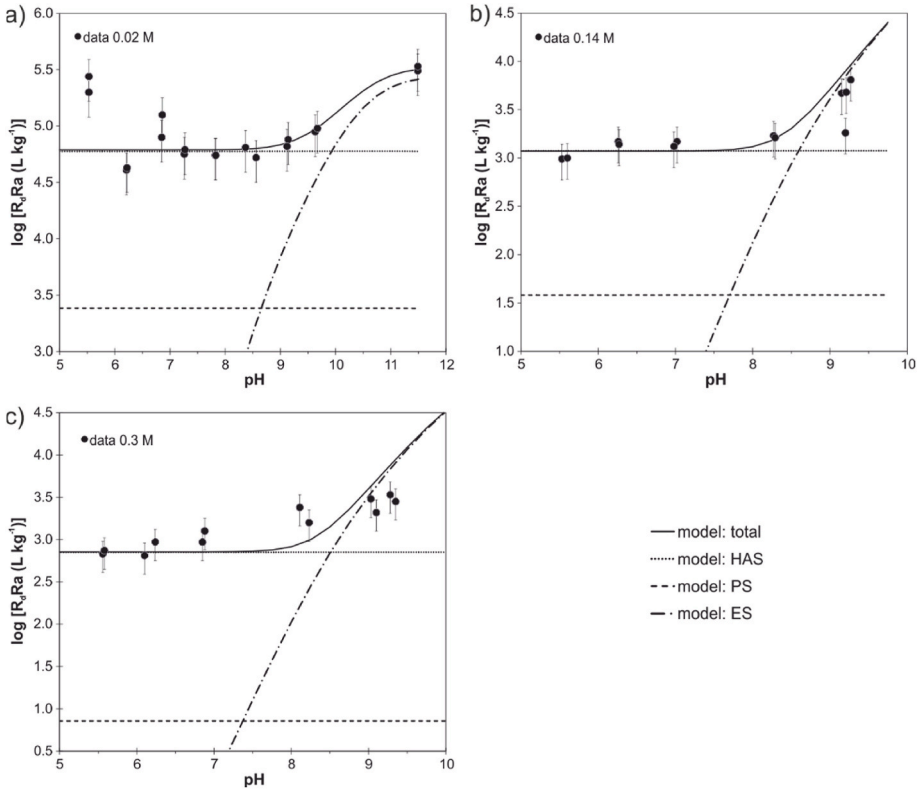

Fig. 3. Experimental and modelling results of pH-edges of ^{226}Ra on Na-IdP in (a) 0.02 M NaCl, (b) 0.14 M NaCl and (c) 0.3 M NaCl.

3.3. Competitive adsorption of Ra and Ba on Na-IdP: experimental and modelling

The adsorption of trace ^{226}Ra as a function of increasing Ba concentrations at 0.02 M NaCl on Na-IdP was investigated to quantify the competitive behaviour between these elements. The Ba adsorption isotherm on Na-IdP in 0.02 M NaCl at pH = 7 (Table 1) was determined separately under the same experimental conditions, using stable ^{137}Ba as a carrier for the ^{226}Ra tracer (Fig. 4, open blue circles). Here, the Ba concentration in the liquid phase after adsorption was analytically determined using ICP-MS.

The isotherm of ^{137}Ba in this experiment is identical within the experimental error with the independently determined ^{133}Ba/^{137}Ba isotherm (Fig. 1) and can be described with the same model parameters given in Table 2. The adsorption of Ra (red squares) as a function of Ba concentration, along the Ba isotherm data is shown in Fig. 4. At [Ba_{eql}] $> 10^{-7}$ M the adsorption of Ra decreases, which can be explained by competitive effects of Ba. If Ba and Ra would not compete at all, the log R_d values of Ra should remain constant at 4.8 L·kg^{-1}, which is experimentally not observed. However, if Ba and Ra were fully competing for the same cation exchange sites, the R_d values for Ra should follow the modelled adsorption of Ba in Fig. 4a (red line), which clearly is not the case. The log R_d values for Ra remain systematically higher compared to the calculated data (up to 0.8 log units) suggesting that Ba and Ra are not fully competing on the HAS. Such a competitive behavior of Ra and Ba was not observed on montmorillonite (Klinkenberg et al., 2021), where only exchange on the planar sites was identified with selectivity coefficient $^{PS}K_c$ (Ba–Ra) = $^{PS}K_c$ (Ra–Na) = 5.

An attempt to model the trace Ra adsorption behaviour is presented in Fig. 4b and 4c. In a first step, an additional cation exchange site, denoted as site-2, with a small capacity of 1 meq·kg^{-1} is introduced. It should be noted that the capacity of this site-2 is a mere fit parameter. In contrary to the capacity of the HAS, this capacity cannot be directly extracted from the experimental data and was therefore taken in the same order of magnitude as *e.g.* the frayed edge site capacity of illite (*e.g.*, Brouwer et al., 1983; Poinssot et al., 1999) to quantitatively describe the data points at [Me_{eql}] $> 10^{-6}$ M in Fig. 4. With a site-2 capacity of 1 meq·kg^{-1} and a log K_c (Ra–Na) = 4.2 the calculated adsorption of Ra on this additional site yields a log R_d value of 4.2 L·kg^{-1}. Since a cation exchange mechanism is postulated these 2 parameters are inversely related as expressed in Eq. (5).

If Ra and Ba would not compete for site-2, the R_d values for Ra should stay constant at any [Ba_{eql}]. This is clearly not the case, since Ra R_d values decrease with increasing Ba concentration ([Ba_{eql}] $> 10^{-6}$ M). This decrease is most obviously caused by competition of Ba with Ra on site-2. Considering Ba exchange on site-2 with log $^{site\text{-}2}K_c$ (Ba–Na) of 1.3 results in a systematically decrease of the Ra adsorption. The dashed red line in Fig. 4b illustrates the contribution of Ra adsorption on site-2. Introducing this additional site-2 for Ra and Ba improves the fit and allows to describe the Ra adsorption up to [Ba_{eql}] $\sim 10^{-3}$ M (Fig. 4b, solid red line). The adsorption of Ra at [Ba_{eql}] $> 10^{-3}$ M however, is not reproduced.

To model the entire Ra adsorption behaviour as a function of increasing Ba concentrations, a third site (site-3) with a capacity of 1 meq·kg^{-1} and a fitted log $^{site\text{-}3}K_c$ (Ra–Na) = 2.3 had to be included. Similar to the modelling on site-2 a competing log $^{site\text{-}3}K_c$ (Ba–Na) = −2.2 is necessary to fully reproduce the Ra adsorption data as shown in Fig. 4c by the red solid line.

Table 5 summarizes the cation exchange site types, site capacities and selectivity coefficients required to model the Ra–Ba competition experiment. From Ba–Na and Ra–Na exchange equilibria, the selectivity coefficients between Ra and Ba can be calculated. The results shown in Table 4 illustrate the following trend for the selectivity coefficients: $^{site\text{-}3}K_c$(Ra–Ba) ≫ $^{site\text{-}2}K_c$(Ra–Ba) ≫ $^{HAS}K_c$(Ra–Ba) > $^{PS}K_c$(Ra–Ba). Finally, the introduction of site-2 and site-3 does not affect the Ba adsorption since the capacity and K_c (Ba–Na) values are much smaller compared

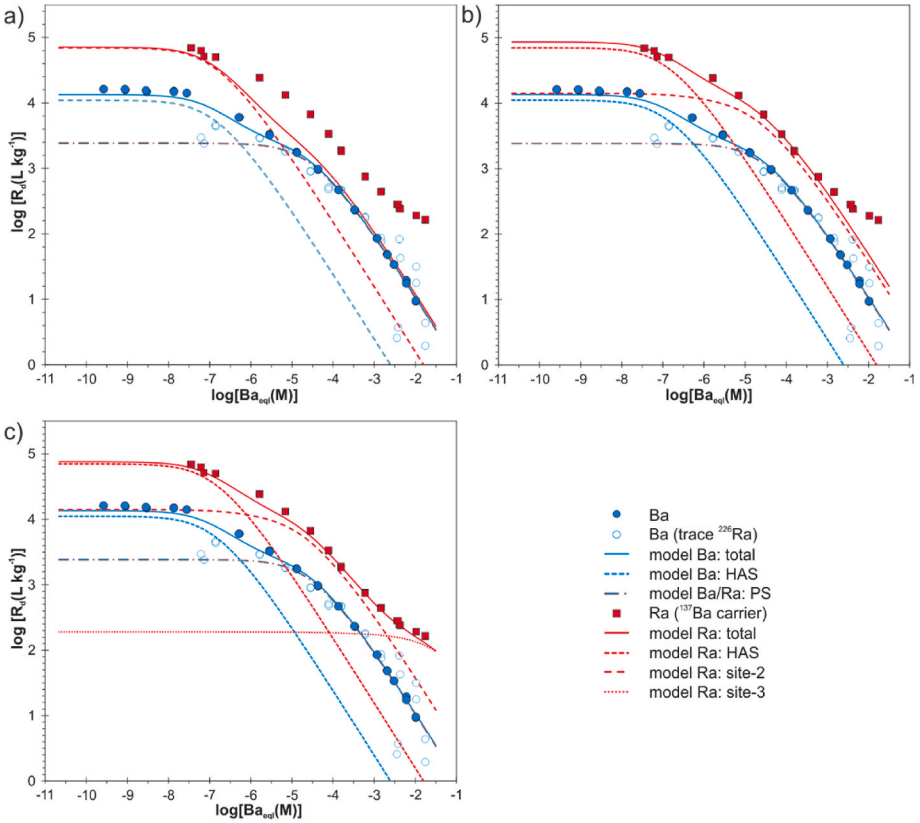

Fig. 4. Experimental and modelled results of ^{226}Ra adsorption in the presence of Ba on Na-IdP in 0.02 M NaCl (see text for details).

Table 5
Summary of site types and capacities and selectivity coefficients required for the modelling of the Ra/Ba competition experiment on Na-IdP at pH 7 in 0.02 M NaCl.

Cation exchange site type	Site capacity ($meq \cdot kg^{-1}$)
Planar sites (PS)	225
High affinity sites (HAS)	5
Site-2	1
Site-3	1
Ba–Na exchange reaction	**log K_c**
2Na-PS + Ba^{2+} ⇔ Ba-PS + $2Na^+$	1.05
2Na-HAS + Ba^{2+} ⇔ Ba-HAS + $2Na^+$	3.4
2Na-site-2 + Ba^{2+} ⇔ Ba-site-2+ $2Na^+$	1.3
2Na-site-3 + Ba^{2+} ⇔ Ba-site-3+ $2Na^+$	−2.2
Ra–Na exchange reaction	**log K_c**
2Na-PS + Ra^{2+} ⇔ Ra-PS + $2Na^+$	1.05
2Na-HAS + Ra^{2+} ⇔ Ra-HAS + $2Na^+$	4.2
2Na-site2 + Ra^{2+} ⇔ Ra-site2+ $2Na^+$	4.2
2Na-site3 + Ra^{2+} ⇔ Ra-site3+ $2Na^+$	2.3
Ra–Ba exchange reaction	**log K_c**
Ba-PS + Ra^{2+} ⇔ Ra-PS + Ba^{2+}	0.0
Ba-HAS + Ra^{2+} ⇔ Ra-HAS + Ba^{2+}	0.8
Ba-site2 + Ra^{2+} ⇔ Ra-site2 + Ba^{2+}	2.9
Ba-site3 + Ra^{2+} ⇔ Ra-site3 + Ba^{2+}	4.5

with the Ba adsorption on HAS and PS. ^{226}Ra adsorption on site-2 and site-3 is modelled as cation exchange but there is no evidence for this mechanism based on the experimental data, the retention could also be due to other processes such as uptake by undetected trace mineral impurities. Onto IdP, Montoya et al. (2018) observed an unexpected adsorption behavior at low pH for trace Zn, which could not be described solely by cation exchange on the planar sites and which also required the consideration of an additional high affinity site.

4. Conclusions

The safety assessment of geological formations for the deep disposal of radioactive waste relies on thermodynamic models capable of predicting the retention of radionuclides on the mineral constituents of heterogeneous rock environments over a wide range of physico-chemical conditions. The aim of this study was to develop a quantitative model for Ba and ^{226}Ra adsorption on a homo-ionic Na illite and to evaluate the suitability of Ba as a chemical analogue for ^{226}Ra.

Our study showed that the adsorption of Ba and Ra on illite follows similar trends. However, in contrast to adsorption on montmorillonite (Klinkenberg et al., 2021), additional high affinity sites (HAS) are present in illite for which Ra shows a higher affinity than Ba.. The Ba adsorption isotherms obtained on Na-IdP at varying pH and fixed ionic strength (0.02 M NaCl) are very similar, exhibiting a non-linear behavior in the Ba equilibrium concentration range of 10^{-7} to 10^{-2} M. The data are well described by cation exchange reactions on two types of adsorption sites, planar and high affinity, with corresponding selectivity coefficients. In addition, to describe the uptake of Ba at high pH, a surface complexation reaction on the amphoteric edge sites was considered with a best-fit surface complexation constant.

In comparison to Ba, pH edges at varying ionic strengths consistently reveal a higher selectivity of ^{226}Ra towards illite. The ^{226}Ra pH edges are well described by similar cation exchange and surface complexation reactions as for Ba. An additional ^{226}Ra–Ba adsorption experiment with Ba intended as a carrier for ^{226}Ra confirmed the stronger affinity of ^{226}Ra. The different behaviour of ^{226}Ra compared to Ba in this experiment could be reproduced by a more complex model, which includes two additional high affinity sites for ^{226}Ra and Ba. The nature of these sites, however, is not clear. We have assumed that these sites are cation exchange sub-sites of HAS, but they could also be due to other processes such as uptake by undetected trace mineral impurities. The identification of these sites or of the retention mechanism at the molecular scale (with *e.g.*, synchrotron techniques) is difficult because it would require much higher amount of adsorbed ^{226}Ra than the amount adsorbed to illite in the competition experiment (~0.1 – 0.15 $mmol \cdot kg^{-1}$ illite).

The newly derived thermodynamic parameters will be integrated into an adsorption model for safety relevant (radio-)contaminants. The correct description of ^{226}Ra, as a daughter nuclide of the long living ^{238}U, adsorption on key soil/rock constituents such as clay minerals as well as its implementation in coupled transport codes is of paramount importance to reduce uncertainties and consequently improve the reliability of the prediction of their long-term transport behavior in argillaceous environments over a wider range of relevant porewater and mineralogical conditions.

Declaration of competing interest

The authors declare the following financial interests/personal relationships which may be considered as potential competing interests: Maria Marques Fernandes reports financial support was provided by European Union.

Data availability

Data are included in the manuscript

Acknowledgements

This project has received funding from the European Union's Horizon 2020 research and innovation programme under grant agreement No 847593 (EURAD WP Future). We are grateful to A. Schaible and M. Güngör for technical assistance.

Appendix

Table A 1
Experimental data of isotherms of Ba sorption at pH 5.1, pH 6.6, and pH 6.9 with I = 0.02 M NaCl (Fig. 1a).

Experimental data					
pH 5.1		pH 6.6		pH 6.9	
log [Ba_{eql}]	log [R_{dl}]	log [Ba_{eql}]	log R_d	log [Ba_{eql}]	log R_d
log (M)	log ($L \cdot kg^{-1}$)	log (M)	log ($L \cdot kg^{-1}$)	log (M)	log ($L \cdot kg^{-1}$)
−2.14	1.22	−1.91	0.94	−1.99	0.97
−2.15	1.24	−1.91	1.01	−1.99	0.98
−2.37	1.42	−2.29	1.23	−2.22	1.27
−2.37	1.40	−2.30	1.46	−2.22	1.21
−2.60	1.65	−2.43	1.46	−2.52	1.55
−2.60	1.64	−2.43	1.50	−2.52	1.55
−2.77	1.79	−2.77	1.80	−2.69	1.67

(*continued on next page*)

Table A 1 (*continued*)

Experimental data					
pH 5.1		pH 6.6		pH 6.9	
log [Ba_{eql}]	log [R_{dl}]	log [Ba_{eql}]	log R_d	log [Ba_{eql}]	log R_d
log (M)	log ($L \cdot kg^{-1}$)	log (M)	log ($L \cdot kg^{-1}$)	log (M)	log ($L \cdot kg^{-1}$)
−2.78	1.80	−2.77	1.84	−2.68	1.66
−2.98	1.98	−3.14	2.16	−2.93	1.87
−2.97	1.97	−3.14	2.15	−2.93	1.88
−3.50	2.41	−3.71	2.56	−3.47	2.37
−3.50	2.41	−3.73	2.61	−3.48	2.37
−3.77	2.60	−4.13	2.88	−3.87	2.66
−3.77	2.60	−4.13	2.88	−3.87	2.66
−4.20	2.86	−4.57	3.12	−4.37	2.98
−4.20	2.86	−4.57	3.11	−4.37	2.99
−4.67	3.11	−5.18	3.37	−4.89	3.24
−4.67	3.11	−5.18	3.37	−4.88	3.23
−5.31	3.37	−5.88	3.63	−5.55	3.50
−5.31	3.36	−5.87	3.62	−5.54	3.50
−5.97	3.57	−7.17	4.04	−6.28	3.77
−5.96	3.56	−7.17	4.04	−6.29	3.77
−7.20	3.90	−7.97	4.17	−7.56	4.13
−7.19	3.89	−7.97	4.16	−7.56	4.13
−7.92	3.95	−8.74	4.26	−7.87	4.18
−7.92	3.95			−7.87	4.17
−8.64	4.00			−8.53	4.17
−8.64	4.00			−8.55	4.19
−9.14	4.03			−9.05	4.20
−9.14	4.02			−9.06	4.21
−9.68	4.06			−9.58	4.21
−9.66	4.03			−9.58	4.21

Table A 2
Experimental data of isotherms of Ba sorption at pH 7.6, pH 9.0, and pH 7.0 (FZJ, trace ^{226}Ra) with I = 0.02 M NaCl (Fig. 1a).

Experimental data					
pH 7.6		pH 9.0		pH 7.0 (FZJ)	
log [Ba_{eql}]	log R_d	log [Ba_{eql}]	log R_d	log [Ba_{eql}]	log R_d
log (M)	log ($L \cdot kg^{-1}$)	log (M)	log ($L \cdot kg^{-1}$)	log (mM)	log ($L \cdot kg^{-1}$)
−2.16	1.33	−2.14	1.11	−1.76	0.29
−2.17	1.36	−2.14	1.10	−1.76	0.64
−2.40	1.56	−2.42	1.36	−1.98	1.50
−2.40	1.55	−2.43	1.38	−1.98	1.25
−2.64	1.78	−2.57	1.52	−2.39	1.92
−2.64	1.78	−2.56	1.50	−2.37	1.63
−2.83	1.95	−2.83	1.76	−2.45	0.41
−2.83	1.94	−2.83	1.75	−2.42	0.57
−3.03	2.12	−3.02	1.94	−2.83	1.88
−3.02	2.11	−3.02	1.95	−2.84	1.94
−3.61	2.59	−3.72	2.46	−3.22	2.24
−3.61	2.59	−3.71	2.46	−3.22	2.26
−3.85	2.77	−3.86	2.57	−3.81	2.67
−3.85	2.76	−3.86	2.57	−3.80	2.67
−4.32	3.05	−4.32	2.86	−4.11	2.68
−4.32	3.05	−4.32	2.85	−4.11	2.71
−4.82	3.30	−4.83	3.10	−4.55	2.95
−4.82	3.30	−4.82	3.09	−4.55	2.96
−5.50	3.59	−5.48	3.33	−5.16	3.26
−5.50	3.59	−5.48	3.33	−5.16	3.26
−6.18	3.80	−6.19	3.58	−5.79	3.47
−6.19	3.81	−6.19	3.58	−5.78	3.46
−7.45	4.16	−7.42	3.87	−6.85	3.64
−7.45	4.16	−7.43	3.87	−6.86	3.66
−8.15	4.19	−8.15	3.95	−7.14	3.38
−8.15	4.19	−8.16	3.96	−7.21	3.47
−8.90	4.27	−8.90	4.02		
−8.90	4.27	−8.89	4.01		
−9.40	4.29	−9.51	4.01		
−9.40	4.29	−9.48	3.99		
−9.91	4.30	−10.43	4.05		
−9.92	4.30	−10.43	4.05		

Table A 3
Modelling data of isotherms of Ba sorption at pH 5.1 – 9.0 with I = 0.02 M NaCl (Fig. 1a).

Modelling ^{226}Ba sorption, pH 5.1 – 9.0			
log [Ba_{eql}]	log $R_{d\ total}$	log $R_{d\ HAS}$	log $R_{d\ PS}$
log (M)	log ($L \cdot kg^{-1}$)		
−10.66	4.16	4.08	3.38
−10.41	4.16	4.08	3.38
−10.16	4.16	4.08	3.38
−9.91	4.16	4.08	3.38
−9.66	4.16	4.08	3.38
−9.41	4.16	4.08	3.38
−9.16	4.16	4.08	3.38
−8.91	4.15	4.07	3.38
−8.66	4.15	4.07	3.38
−8.41	4.15	4.06	3.38
−8.16	4.14	4.05	3.38
−7.91	4.12	4.03	3.38
−7.66	4.09	4.00	3.38
−7.41	4.05	3.95	3.38
−7.16	4.00	3.88	3.38
−6.91	3.92	3.78	3.38
−6.66	3.84	3.65	3.38
−6.41	3.74	3.50	3.38
−6.16	3.65	3.33	3.37
−5.91	3.56	3.13	3.36
−5.66	3.49	2.93	3.35
−5.41	3.41	2.71	3.32
−5.16	3.34	2.49	3.28
−4.91	3.26	2.25	3.21
−4.66	3.16	2.02	3.12
−4.41	3.03	1.78	3.01
−4.16	2.88	1.54	2.86
−3.91	2.72	1.29	2.70
−3.66	2.53	1.05	2.51
−3.41	2.32	0.80	2.31
−3.16	2.11	0.55	2.10
−2.90	1.88	0.29	1.87
−2.64	1.64	0.04	1.63
−2.38	1.39	−0.23	1.38
−2.10	1.13	−0.50	1.12
−1.81	0.85	−0.79	0.84
−1.50	0.55	−1.10	0.54

Table A 4
Experimental data of isotherms of Ba sorption at pH 5.1, pH 6.6, and pH 6.9 with I = 0.02 M NaCl (Fig. 1b).

Experimental data					
pH 5.1		pH 6.6		pH 6.9	
log [Ba_{eql}]	log [Ba_{ads}]	log [Ba_{eql}]	log [Ba_{ads}]	log [Ba_{eql}]	log [Ba_{ads}]
log (M)	log ($mol\ kg^{-1}$)	log (M)	log ($mol \cdot kg^{-1}$)	log (M)	log ($mol \cdot kg^{-1}$)
−2.14	−0.92	−1.91	−0.97	−1.99	−1.02
−2.15	−0.91	−1.91	−0.90	−1.99	−1.01
−2.37	−0.95	−2.29	−1.06	−2.22	−0.95
−2.37	−0.97	−2.30	−0.84	−2.22	−1.01
−2.60	−0.95	−2.43	−0.97	−2.52	−0.97
−2.60	−0.96	−2.43	−0.93	−2.52	−0.97
−2.77	−0.98	−2.77	−0.97	−2.69	−1.02
−2.78	−0.98	−2.77	−0.93	−2.68	−1.02
−2.98	−1.00	−3.14	−0.98	−2.93	−1.06
−2.97	−1.00	−3.14	−0.99	−2.93	−1.05
−3.50	−1.09	−3.71	−1.15	−3.47	−1.10
−3.50	−1.09	−3.73	−1.12	−3.48	−1.11
−3.77	−1.17	−4.13	−1.25	−3.87	−1.21
−3.77	−1.17	−4.13	−1.25	−3.87	−1.21
−4.20	−1.34	−4.57	−1.45	−4.37	−1.39
−4.20	−1.34	−4.57	−1.46	−4.37	−1.38
−4.67	−1.56	−5.18	−1.81	−4.89	−1.65
−4.67	−1.56	−5.18	−1.81	−4.88	−1.65
−5.31	−1.94	−5.88	−2.25	−5.55	−2.05
−5.31	−1.95	−5.87	−2.25	−5.54	−2.04
−5.97	−2.40	−7.17	−3.13	−6.28	−2.51

(*continued on next page*)

Table A 4 (*continued*)

Experimental data					
pH 5.1		pH 6.6		pH 6.9	
log [Ba_{eql}]	log [Ba_{ads}]	log [Ba_{eql}]	log [Ba_{ads}]	log [Ba_{eql}]	log [Ba_{ads}]
log (M)	log (mol kg^{-1})	log (M)	log (mol·kg^{-1})	log (M)	log (mol·kg^{-1})
−5.96	−2.40	−7.17	−3.13	−6.29	−2.52
−7.20	−3.30	−7.97	−3.80	−7.56	−3.43
−7.19	−3.30	−7.97	−3.81	−7.56	−3.43
−7.92	−3.97	−8.74	−4.48	−7.87	−3.69
−7.92	−3.97			−7.87	−3.70
−8.64	−4.64			−8.53	−4.36
−8.64	−4.64			−8.55	−4.36
−9.14	−5.11			−9.05	−4.85
−9.14	−5.12			−9.06	−4.85
−9.68	−5.62			−9.58	−5.37
−9.66	−5.63			−9.58	−5.37

Table A 5
Experimental data of isotherms of Ba sorption at pH 7.6, pH 9.0, and pH 7.0 (FZJ, trace ^{226}Ra) with I = 0.02 mol·L^{-1} NaCl (Fig. 1).

Experimental data					
pH 7.6		pH 9.0		pH 7.0 (FZJ)	
log [Ba_{eql}]	log [Ba_{ads}]	log [Ba_{eql}]	log [Ba_{ads}]	log [Ba_{eql}]	log [Ba_{ads}]
log (mol·L^{-1})	log (mol·kg^{-1})	log (mol·L^{-1})	log (mol·kg^{-1})	log (mol·L^{-1})	log (mol·kg^{-1})
−2.16	−0.83	−2.14	−1.03	−1.76	−1.47
−2.17	−0.81	−2.14	−1.04	−1.76	−1.12
−2.40	−0.84	−2.42	−1.06	−1.98	−0.48
−2.40	−0.85	−2.43	−1.05	−1.98	−0.73
−2.64	−0.86	−2.57	−1.05	−2.39	−0.47
−2.64	−0.86	−2.56	−1.06	−2.37	−0.74
−2.83	−0.88	−2.83	−1.07	−2.45	−2.04
−2.83	−0.89	−2.83	−1.08	−2.42	−1.85
−3.03	−0.91	−3.02	−1.08	−2.83	−0.95
−3.02	−0.91	−3.02	−1.07	−2.84	−0.90
−3.61	−1.02	−3.72	−1.26	−3.22	−0.98
−3.61	−1.02	−3.71	−1.25	−3.22	−0.96
−3.85	−1.08	−3.86	−1.29	−3.81	−1.14
−3.85	−1.09	−3.86	−1.29	−3.80	−1.13
−4.32	−1.27	−4.32	−1.46	−4.11	−1.43
−4.32	−1.27	−4.32	−1.47	−4.11	−1.40
−4.82	−1.52	−4.83	−1.73	−4.55	−1.60
−4.82	−1.52	−4.82	−1.73	−4.55	−1.59
−5.50	−1.91	−5.48	−2.15	−5.16	−1.90
−5.50	−1.91	−5.48	−2.15	−5.16	−1.90
−6.18	−2.38	−6.19	−2.61	−5.79	−2.32
−6.19	−2.38	−6.19	−2.61	−5.78	−2.32
−7.45	−3.29	−7.42	−3.55	−6.85	−3.21
−7.45	−3.29	−7.43	−3.56	−6.86	−3.20
−8.15	−3.96	−8.15	−4.20	−7.14	−3.76
−8.15	−3.96	−8.16	−4.20	−7.21	−3.74
−8.90	−4.63	−8.90	−4.88		
−8.90	−4.63	−8.89	−4.88		
−9.40	−5.11	−9.51	−5.50		
−9.40	−5.11	−9.48	−5.49		
−9.91	−5.61	−10.43	−6.38		
−9.92	−5.62	−10.43	−6.38		

Table A 6
Modelling data of isotherms of Ba sorption at pH 5.1–9.0 with I = 0.02 M NaCl (Fig. 1b).

Modelling ^{226}Ba sorption, pH 5.1–9.0			
log [Ba_{eql}]	log $R_{d\ total}$	log $R_{d\ HAS}$	log $R_{d\ PS}$
log M)	log (L·kg^{-1})		
−10.66	−6.51	−6.59	−7.28
−10.41	−6.26	−6.34	−7.03
−10.16	−6.01	−6.09	−6.78

(*continued on next page*)

Table A 6 (*continued*)

Modelling ^{226}Ba sorption, pH 5.1–9.0			
log [Ba_{eql}]	log $R_{d\ total}$	log $R_{d\ HAS}$	log $R_{d\ PS}$
log M)	log ($L{\cdot}kg^{-1}$)		
−9.91	−5.76	−5.84	−6.53
−9.66	−5.51	−5.59	−6.28
−9.41	−5.26	−5.34	−6.03
−9.16	−5.01	−5.09	−5.78
−8.91	−4.76	−4.84	−5.53
−8.66	−4.51	−4.60	−5.28
−8.41	−4.27	−4.35	−5.03
−8.16	−4.03	−4.11	−4.78
−7.91	−3.79	−3.88	−4.53
−7.66	−3.57	−3.66	−4.28
−7.41	−3.36	−3.46	−4.03
−7.16	−3.17	−3.29	−3.78
−6.91	−2.99	−3.14	−3.53
−6.66	−2.83	−3.01	−3.28
−6.41	−2.67	−2.92	−3.04
−6.16	−2.51	−2.84	−2.79
−5.91	−2.35	−2.78	−2.55
−5.66	−2.18	−2.74	−2.32
−5.41	−2.00	−2.70	−2.10
−5.16	−1.82	−2.68	−1.89
−4.91	−1.66	−2.66	−1.70
−4.66	−1.51	−2.64	−1.54
−4.41	−1.38	−2.63	−1.41
−4.16	−1.28	−2.63	−1.30
−3.91	−1.20	−2.62	−1.21
−3.66	−1.13	−2.62	−1.15
−3.41	−1.09	−2.61	−1.10
−3.16	−1.05	−2.61	−1.06
−2.90	−1.02	−2.61	−1.03
−2.64	−1.00	−2.61	−1.01
−2.38	−0.99	−2.61	−1.00
−2.10	−0.97	−2.60	−0.98
−1.81	−0.96	−2.60	−0.97
−1.50	−0.96	−2.60	−0.97

Table A 7
Experimental and modelling data of pH edges of Ba sorption at with I = 0.02 M NaCl (Fig. 2a).

Experimental data		Modelling				
pH	log R_d	pH	log $R_{d\ total}$	log $R_{d\ HAS}$	log $R_{d\ PS}$	log $R_{d\ W2}$
	log ($L{\cdot}kg^{-1}$)		log ($L{\cdot}kg^{-1}$)			
5.09	3.97	5.00	4.16	4.08	3.38	−4.53
5.10	3.96	5.25	4.16	4.08	3.38	−4.03
5.91	4.03	5.50	4.16	4.08	3.38	−3.53
5.93	4.02	5.75	4.16	4.08	3.38	−3.03
6.45	4.07	6.00	4.16	4.08	3.38	−2.54
6.48	4.07	6.25	4.16	4.08	3.38	−2.04
7.34	4.13	6.50	4.16	4.08	3.38	−1.54
7.36	4.12	6.75	4.16	4.08	3.38	−1.04
7.76	4.09	7.00	4.16	4.08	3.38	−0.55
7.75	4.09	7.25	4.16	4.08	3.38	−0.06
8.39	4.20	7.50	4.16	4.08	3.38	0.42
8.40	4.20	7.75	4.16	4.08	3.38	0.90
9.14	4.30	8.00	4.16	4.08	3.38	1.35
9.13	4.29	8.25	4.16	4.08	3.38	1.77
9.77	4.39	8.50	4.16	4.08	3.38	2.16
9.76	4.38	8.75	4.17	4.08	3.38	2.52
10.85	4.48	9.00	4.18	4.08	3.38	2.84
10.85	4.48	9.25	4.19	4.08	3.38	3.12
		9.50	4.22	4.08	3.38	3.39
		9.75	4.27	4.08	3.38	3.62
		10.00	4.33	4.08	3.38	3.84
		10.25	4.39	4.08	3.38	4.02
		10.50	4.46	4.08	3.38	4.16
		10.75	4.52	4.08	3.38	4.27
		11.00	4.56	4.08	3.38	4.34

Table A 8
Experimental and modelling data of pH edges of Ba sorption at with I = 0.03 M NaCl (Fig. 2b).

Experimental data		Modelling				
pH	log R_d	pH	log $R_{d\ total}$	log $R_{d\ HAS}$	log $R_{d\ PS}$	log $R_{d\ W2}$
	log ($L{\cdot}kg^{-1}$)		log ($L{\cdot}kg^{-1}$)			
5.45	3.69	5.00	4.04	4.00	3.01	−4.58
5.44	3.71	5.25	4.04	4.00	3.01	−4.08
6.11	3.82	5.50	4.04	4.00	3.01	−3.58
6.10	3.82	5.75	4.04	4.00	3.01	−3.08
6.58	3.88	6.00	4.04	4.00	3.01	−2.58
6.61	3.88	6.25	4.04	4.00	3.01	−2.08
7.14	3.99	6.50	4.04	4.00	3.01	−1.58
7.14	3.98	6.75	4.04	4.00	3.01	−1.08
7.64	3.90	7.00	4.04	4.00	3.01	−0.59
7.66	3.91	7.25	4.04	4.00	3.01	−0.10
8.25	4.07	7.50	4.04	4.00	3.01	0.38
8.28	4.07	7.75	4.04	4.00	3.01	0.85
8.75	4.22	8.00	4.05	4.00	3.01	1.31
8.73	4.23	8.25	4.05	4.00	3.01	1.73
9.30	4.38	8.50	4.05	4.00	3.01	2.12
9.25	4.38	8.75	4.06	4.00	3.01	2.48
7.60	4.16	9.00	4.07	4.00	3.01	2.80
7.63	4.16	9.25	4.09	4.00	3.01	3.08
		9.50	4.12	4.00	3.01	3.35
		9.75	4.17	4.00	3.01	3.58
		10.00	4.24	4.00	3.01	3.79
		10.25	4.31	4.00	3.01	3.98
		10.50	4.39	4.00	3.01	4.12
		10.75	4.45	4.00	3.01	4.23
		11.00	4.49	4.00	3.01	4.30

Table A 9
Experimental and modelling data of pH edges of Ba sorption at with I = 0.3 M NaCl (Fig. 2c).

Experimental data		Modelling				
pH	log R_d	pH	log $R_{d\ total}$	log $R_{d\ HAS}$	log $R_{d\ PS}$	log $R_{d\ W2}$
	log ($L{\cdot}kg^{-1}$)		log ($L{\cdot}kg^{-1}$)			
5.48	2.28	5.00	2.49	2.48	0.89	−4.83
5.49	2.27	5.25	2.49	2.48	0.89	−4.33
6.12	2.40	5.50	2.49	2.48	0.89	−3.83
6.13	2.38	5.75	2.49	2.48	0.89	−3.33
6.65	2.49	6.00	2.49	2.48	0.89	−2.83
6.68	2.48	6.25	2.49	2.48	0.89	−2.33
7.10	2.55	6.50	2.49	2.48	0.89	−1.83
7.15	2.55	6.75	2.49	2.48	0.89	−1.33
7.57	2.63	7.00	2.49	2.48	0.89	−0.84
7.60	2.62	7.25	2.49	2.48	0.89	−0.35
8.15	2.77	7.50	2.49	2.48	0.89	0.13
8.17	2.79	7.75	2.50	2.48	0.89	0.60
8.81	2.96	8.00	2.51	2.48	0.89	1.05
8.81	2.97	8.25	2.53	2.48	0.89	1.48
9.29	3.11	8.50	2.58	2.48	0.89	1.87
9.27	3.15	8.75	2.68	2.48	0.89	2.23
8.51	2.89	9.00	2.82	2.48	0.89	2.54
8.50	2.90	9.25	3.00	2.48	0.89	2.83
9.91	3.40	9.50	3.19	2.48	0.89	3.10
9.94	3.41	9.75	3.39	2.48	0.89	3.33
10.56	3.74	10.00	3.58	2.48	0.89	3.54
10.54	3.74	10.25	3.75	2.48	0.89	3.73
		10.50	3.89	2.48	0.89	3.87
		10.75	3.99	2.48	0.89	3.98
		11.00	4.07	2.48	0.89	4.05

Table A 10
Experimental and modelling results of pH-edges of ^{226}Ra on Na-IdP in 0.02 M NaCl (Fig. 3a).

Experimental data		Modelling				
pH	log R_d	pH	log $R_{d\ total}$	log $R_{d\ HAS}$	log $R_{d\ PS}$	log $R_{d\ W2}$
	log ($L \cdot kg^{-1}$)		log ($L \cdot kg^{-1}$)			
5.53	5.30	5.00	4.79	4.77	3.38	−3.53
5.53	5.44	5.25	4.79	4.77	3.38	−3.03
6.21	4.61	5.50	4.79	4.77	3.38	−2.53
6.22	4.63	5.75	4.79	4.77	3.38	−2.03
6.85	4.90	6.00	4.79	4.77	3.38	−1.54
6.86	5.10	6.25	4.79	4.77	3.38	−1.04
7.26	4.75	6.50	4.79	4.77	3.38	−0.54
7.27	4.79	6.75	4.79	4.77	3.38	−0.04
7.82	4.74	7.00	4.79	4.77	3.38	0.45
7.83	4.74	7.25	4.79	4.77	3.38	0.94
8.56	4.72	7.50	4.79	4.77	3.38	1.42
8.37	4.81	7.75	4.79	4.77	3.38	1.90
9.14	4.88	8.00	4.79	4.77	3.38	2.35
9.12	4.82	8.25	4.79	4.77	3.38	2.77
9.63	4.95	8.50	4.80	4.77	3.38	3.16
9.67	4.98	8.75	4.81	4.77	3.38	3.52
11.49	5.49	9.00	4.83	4.78	3.38	3.84
11.49	5.53	9.25	4.87	4.78	3.38	4.12
		9.50	4.93	4.78	3.38	4.39
		9.75	5.01	4.78	3.38	4.62
		10.00	5.11	4.78	3.38	4.84
		10.25	5.22	4.78	3.38	5.02
		10.50	5.31	4.78	3.38	5.16
		10.75	5.39	4.78	3.38	5.27
		11.00	5.45	4.78	3.38	5.34
		11.25	5.48	4.78	3.38	5.39
		11.50	5.50	4.77	3.38	5.42

Table A 11
Experimental and modelling results of pH-edges of ^{226}Ra on Na-IdP in 0.14 M NaCl (Fig. 3b).

Experimental data		Modelling				
pH	log R_d	pH	log $R_{d\ total}$	log $R_{d\ HAS}$	log $R_{d\ PS}$	log $R_{d\ W2}$
	log ($L \cdot kg^{-1}$)		log ($L \cdot kg^{-1}$)			
5.53	2.99	5.00	3.07	3.07	1.58	−3.76
5.60	3.00	5.25	3.07	3.07	1.58	−3.26
6.26	3.17	5.50	3.07	3.07	1.58	−2.76
6.27	3.14	5.75	3.07	3.07	1.58	−2.26
7.02	3.17	6.00	3.07	3.07	1.58	−1.76
6.98	3.12	6.25	3.07	3.07	1.58	−1.26
8.27	3.23	6.50	3.07	3.07	1.58	−0.76
8.29	3.21	6.75	3.07	3.07	1.58	−0.27
9.15	3.67	7.00	3.07	3.07	1.58	0.23
9.20	3.26	7.25	3.07	3.07	1.58	0.72
9.21	3.68	7.50	3.08	3.07	1.58	1.20
9.27	3.81	7.75	3.09	3.07	1.58	1.67
		8.00	3.12	3.07	1.58	2.12
		8.25	3.18	3.07	1.58	2.55
		8.50	3.30	3.07	1.58	2.94
		8.75	3.49	3.07	1.58	3.29
		9.00	3.71	3.07	1.58	3.61
		9.25	3.95	3.07	1.58	3.90
		9.50	4.18	3.08	1.58	4.16
		9.75	4.40	3.08	1.58	4.40

Table A 12
Experimental and modelling results of pH-edges of ^{226}Ra on Na-IdP in 0.3 M NaCl (Fig. 3c).

Experimental data		Modelling				
pH	log R_d	pH	log $R_{d\ total}$	log $R_{d\ HAS}$	log $R_{d\ PS}$	log $R_{d\ W2}$
	log ($L \cdot kg^{-1}$)		log ($L \cdot kg^{-1}$)			
5.56	2.83	4.50	2.85	2.85	0.86	−4.86

(*continued on next page*)

Table A 12 (*continued*)

Experimental data		Modelling				
pH	log R_d	pH	log $R_{d\ total}$	log $R_{d\ HAS}$	log $R_{d\ PS}$	log $R_{d\ W2}$
	log ($L \cdot kg^{-1}$)		log ($L \cdot kg^{-1}$)			
5.58	2.87	4.75	2.85	2.85	0.86	−4.36
6.10	2.81	5.00	2.85	2.85	0.86	−3.86
6.24	2.97	5.25	2.85	2.85	0.86	−3.36
6.85	2.97	5.50	2.85	2.85	0.86	−2.86
6.88	3.10	5.75	2.85	2.85	0.86	−2.36
8.23	3.20	6.00	2.85	2.85	0.86	−1.86
8.11	3.38	6.25	2.85	2.85	0.86	−1.36
9.10	3.32	6.50	2.85	2.85	0.86	−0.86
9.03	3.48	6.75	2.85	2.85	0.86	−0.36
9.28	3.53	7.00	2.85	2.85	0.86	0.13
9.35	3.45	7.25	2.86	2.85	0.86	0.62
		7.50	2.86	2.85	0.86	1.10
		7.75	2.88	2.85	0.86	1.57
		8.00	2.91	2.85	0.86	2.02
		8.25	3.00	2.85	0.86	2.45
		8.50	3.15	2.85	0.86	2.84
		8.75	3.36	2.85	0.86	3.20
		9.00	3.60	2.85	0.86	3.51
		9.25	3.85	2.85	0.86	3.80
		9.50	4.09	2.85	0.86	4.07
		9.75	4.32	2.85	0.86	4.30
		10.00	4.52	2.85	0.86	4.51

Table A 13
Experimental data of Ba and ^{226}Ra adsorption in the presence of Ba on Na-IdP in 0.02 M NaCl at pH 7 (Fig. 4a,b,c).

Experimental data				
Ba isotherm		Ba (trace ^{226}Ra)		^{226}Ra (^{137}Ba carrier)
log [Ba_{eql}]	log R_d	log [Ba_{eql}]	log R_d	log R_d
log (M)	log ($L \cdot kg^{-1}$)	log (M)	log ($L \cdot kg^{-1}$)	log ($L \cdot kg^{-1}$)
−1.99	0.97	−1.76	0.29	2.21
−1.99	0.98	−1.76	0.64	2.22
−2.22	1.29	−1.98	1.50	2.28
−2.22	1.24	−1.98	1.25	2.28
−2.52	1.53	−2.39	1.92	2.39
−2.52	1.53	−2.37	1.63	2.38
−2.69	1.69	−2.45	0.41	2.45
−2.68	1.68	−2.42	0.57	2.45
−2.93	1.93	−2.83	1.88	2.65
−2.93	1.93	−2.84	1.94	2.64
−3.47	2.36	−3.22	2.24	2.88
−3.48	2.37	−3.22	2.26	2.87
−3.87	2.67	−3.81	2.67	3.28
−3.87	2.67	−3.80	2.67	3.26
−4.37	2.98	−4.11	2.68	3.52
−4.37	2.99	−4.11	2.71	3.53
−4.89	3.25	−4.55	2.95	3.82
−4.88	3.24	−4.55	2.96	3.83
−5.55	3.52	−5.16	3.26	4.12
−5.54	3.51	−5.16	3.26	4.12
−6.28	3.78	−5.79	3.47	4.39
−6.29	3.78	−5.78	3.46	4.38
−7.56	4.15	−6.85	3.64	4.70
−7.56	4.15	−6.86	3.66	4.70
−7.87	4.18	−7.14	3.38	4.71
−7.87	4.17	−7.21	3.47	4.80
−8.53	4.17	−7.46		4.84
−8.55	4.19	−7.44		4.84
−9.05	4.2			
−9.06	4.21			
−9.58	4.21			
−9.58	4.21			

Table A 14
Modelling data of Ba and ^{226}Ra adsorption in the presence of Ba on Na-IdP in 0.02 M NaCl at pH 7 (Fig. 4a).

Modelling						
Ba isotherm				Ra adsorption (log R_d)		
log [Ba_{eql}]	log $R_{d\ Ba\ total}$	log $R_{d\ Ba\ HAS}$	log $R_{d\ Ba\ PS}$	log [Ra_{eql}]	log $R_{d\ Ra\ HAS}$	log $R_{d\ Ra\ PS}$
log (M)	log ($L{\cdot}kg^{-1}$)			log (M)	log ($L{\cdot}kg^{-1}$)	
−10.66	4.13	4.04	3.38	4.85	4.84	3.38
−10.41	4.13	4.04	3.38	4.85	4.84	3.38
−10.16	4.13	4.04	3.38	4.85	4.84	3.38
−9.91	4.13	4.04	3.38	4.85	4.84	3.38
−9.66	4.13	4.04	3.38	4.85	4.84	3.38
−9.41	4.13	4.04	3.38	4.85	4.84	3.38
−9.16	4.13	4.04	3.38	4.85	4.84	3.38
−8.91	4.12	4.04	3.38	4.85	4.84	3.38
−8.66	4.12	4.03	3.38	4.84	4.83	3.38
−8.41	4.12	4.03	3.38	4.84	4.83	3.38
−8.16	4.11	4.02	3.38	4.83	4.82	3.38
−7.91	4.09	4.00	3.38	4.81	4.80	3.38
−7.66	4.07	3.97	3.38	4.78	4.77	3.38
−7.41	4.03	3.92	3.38	4.73	4.72	3.38
−7.16	3.98	3.85	3.38	4.67	4.65	3.38
−6.91	3.91	3.75	3.38	4.57	4.55	3.38
−6.66	3.82	3.63	3.38	4.46	4.43	3.38
−6.41	3.73	3.48	3.38	4.32	4.28	3.38
−6.16	3.64	3.31	3.37	4.18	4.11	3.37
−5.91	3.56	3.12	3.36	4.02	3.92	3.36
−5.66	3.48	2.91	3.35	3.86	3.71	3.35
−5.41	3.41	2.70	3.32	3.72	3.50	3.32
−5.16	3.34	2.48	3.28	3.57	3.28	3.28
−4.91	3.26	2.25	3.21	3.44	3.05	3.21
−4.66	3.16	2.01	3.12	3.29	2.81	3.12
−4.41	3.03	1.78	3.01	3.14	2.58	3.01
−4.16	2.88	1.53	2.86	2.97	2.34	2.86
−3.91	2.72	1.29	2.70	2.79	2.09	2.70
−3.66	2.53	1.05	2.51	2.59	1.85	2.51
−3.41	2.32	0.80	2.31	2.38	1.60	2.31
−3.16	2.11	0.55	2.10	2.16	1.35	2.10
−2.90	1.88	0.29	1.87	1.93	1.09	1.87
−2.64	1.64	0.04	1.63	1.69	0.84	1.63
−2.38	1.39	−0.23	1.38	1.44	0.57	1.38
−2.10	1.13	−0.50	1.12	1.18	0.30	1.12
−1.81	0.85	−0.79	0.84	0.89	0.01	0.84
−1.50	0.54	−1.10	0.54	0.59	−0.30	0.54

Table A 15
Modelling data of Ba and ^{226}Ra adsorption in the presence of Ba on Na-IdP in 0.02 M NaCl at pH 7 (Fig. 4b).

Modelling							
Ba isotherm				Ra adsorption (log R_d)			
log [Ba_{eql}]	log R_d Ba total	log R_d Ba HAS	log R_d Ba PS	log [Ra_{eql}]	log R_d Ra HAS	log R_d Ra PS	log R_d Ra site 2
log (M)	log ($L{\cdot}kg^{-1}$)			log (M)	log ($L{\cdot}kg^{-1}$)		
−10.66	4.13	4.05	3.38	4.93	4.85	3.38	4.15
−10.41	4.13	4.05	3.38	4.93	4.85	3.38	4.15
−10.16	4.13	4.05	3.38	4.93	4.85	3.38	4.15
−9.91	4.13	4.05	3.38	4.93	4.85	3.38	4.15
−9.66	4.13	4.05	3.38	4.93	4.85	3.38	4.15
−9.41	4.13	4.05	3.38	4.93	4.85	3.38	4.15
−9.16	4.13	4.04	3.38	4.93	4.84	3.38	4.15
−8.91	4.13	4.04	3.38	4.93	4.84	3.38	4.15
−8.66	4.13	4.04	3.38	4.93	4.84	3.38	4.15
−8.41	4.12	4.03	3.38	4.92	4.83	3.38	4.15
−8.16	4.11	4.02	3.38	4.91	4.82	3.38	4.15
−7.91	4.10	4.00	3.38	4.90	4.80	3.38	4.15
−7.66	4.07	3.97	3.38	4.87	4.77	3.38	4.14
−7.41	4.03	3.92	3.38	4.84	4.72	3.38	4.14
−7.16	3.98	3.85	3.38	4.78	4.65	3.38	4.14
−6.91	3.91	3.76	3.38	4.71	4.56	3.38	4.13
−6.66	3.83	3.63	3.38	4.63	4.43	3.38	4.11
−6.41	3.74	3.48	3.38	4.53	4.28	3.38	4.10

(*continued on next page*)

Table A 15 (*continued*)

Modelling							
Ba isotherm				Ra adsorption (log R_d)			
log [Ba_{eql}]	log R_d Ba total	log R_d Ba HAS	log R_d Ba PS	log [Ra_{eql}]	log R_d Ra HAS	log R_d Ra PS	log R_d Ra site 2
log (M)	log ($L \cdot kg^{-1}$)			log (M)	log ($L \cdot kg^{-1}$)		
−6.16	3.65	3.31	3.37	4.43	4.11	3.37	4.08
−5.91	3.56	3.13	3.36	4.34	3.93	3.36	4.05
−5.66	3.49	2.92	3.35	4.25	3.72	3.35	4.01
−5.41	3.42	2.71	3.32	4.16	3.51	3.32	3.96
−5.16	3.34	2.48	3.28	4.07	3.28	3.28	3.90
−4.91	3.26	2.25	3.21	3.97	3.05	3.21	3.82
−4.66	3.16	2.02	3.12	3.85	2.82	3.12	3.71
−4.41	3.03	1.78	3.01	3.71	2.58	3.01	3.58
−4.16	2.89	1.54	2.86	3.55	2.34	2.86	3.42
−3.91	2.72	1.29	2.70	3.37	2.09	2.70	3.25
−3.66	2.53	1.05	2.51	3.18	1.85	2.51	3.06
−3.41	2.33	0.80	2.31	2.98	1.60	2.31	2.85
−3.16	2.11	0.55	2.10	2.76	1.35	2.10	2.64
−2.90	1.88	0.29	1.87	2.54	1.09	1.87	2.42
−2.64	1.64	0.04	1.63	2.30	0.84	1.63	2.18
−2.38	1.39	−0.23	1.38	2.05	0.57	1.38	1.93
−2.10	1.13	−0.50	1.12	1.79	0.30	1.12	1.67
−1.81	0.85	−0.79	0.84	1.51	0.01	0.84	1.39
−1.50	0.55	−1.10	0.54	1.20	−0.30	0.54	1.09

Table A 16
Modelling data of Ba and ^{226}Ra adsorption in the presence of Ba on Na-IdP in 0.02 M NaCl at pH 7 (Fig. 4c).

Modelling								
Ba isotherm				Ra adsorption (log R_d)				
log [Ba_{eql}]	log R_d Ba total	log R_d Ba HAS	log R_d Ba PS	log [Ra_{eql}]	log R_d Ra HAS	log R_d Ra PS	log R_d Ra site 2	log R_d Ra site 3
log (M)	log ($L \cdot kg^{-1}$)			log (M)	log ($L \cdot kg^{-1}$)			
−10.66	4.13	4.05	3.38	4.94	4.85	3.38	4.15	2.28
−10.41	4.13	4.05	3.38	4.94	4.85	3.38	4.15	2.28
−10.16	4.13	4.05	3.38	4.94	4.85	3.38	4.15	2.28
−9.91	4.13	4.05	3.38	4.94	4.85	3.38	4.15	2.28
−9.66	4.13	4.05	3.38	4.94	4.85	3.38	4.15	2.28
−9.41	4.13	4.05	3.38	4.93	4.85	3.38	4.15	2.28
−9.16	4.13	4.04	3.38	4.93	4.84	3.38	4.15	2.28
−8.91	4.13	4.04	3.38	4.93	4.84	3.38	4.15	2.28
−8.66	4.13	4.04	3.38	4.93	4.84	3.38	4.15	2.28
−8.41	4.12	4.03	3.38	4.92	4.83	3.38	4.15	2.28
−8.16	4.11	4.02	3.38	4.91	4.82	3.38	4.15	2.28
−7.91	4.10	4.00	3.38	4.90	4.80	3.38	4.15	2.28
−7.66	4.07	3.97	3.38	4.88	4.77	3.38	4.14	2.28
−7.41	4.03	3.92	3.38	4.84	4.72	3.38	4.14	2.28
−7.16	3.98	3.85	3.38	4.78	4.65	3.38	4.14	2.28
−6.91	3.91	3.76	3.38	4.71	4.56	3.38	4.13	2.28
−6.66	3.83	3.63	3.38	4.63	4.43	3.38	4.11	2.28
−6.41	3.74	3.49	3.38	4.53	4.29	3.38	4.10	2.28
−6.16	3.65	3.31	3.37	4.44	4.11	3.37	4.08	2.28
−5.91	3.56	3.13	3.36	4.34	3.93	3.36	4.05	2.28
−5.66	3.49	2.92	3.35	4.25	3.72	3.35	4.01	2.28
−5.41	3.42	2.71	3.32	4.16	3.51	3.32	3.97	2.28
−5.16	3.34	2.48	3.28	4.08	3.28	3.28	3.90	2.28
−4.91	3.26	2.25	3.21	3.98	3.05	3.21	3.82	2.27
−4.66	3.16	2.02	3.12	3.86	2.82	3.12	3.71	2.27
−4.41	3.03	1.78	3.01	3.73	2.58	3.01	3.58	2.27
−4.16	2.89	1.54	2.86	3.57	2.34	2.86	3.42	2.27
−3.91	2.72	1.29	2.70	3.41	2.09	2.70	3.25	2.26
−3.66	2.53	1.05	2.51	3.23	1.85	2.51	3.06	2.26
−3.41	2.33	0.80	2.31	3.05	1.60	2.31	2.86	2.25
−3.16	2.11	0.55	2.10	2.88	1.35	2.10	2.64	2.24
−2.90	1.88	0.29	1.87	2.71	1.09	1.87	2.42	2.23
−2.64	1.64	0.04	1.63	2.56	0.84	1.63	2.18	2.22
−2.38	1.39	−0.23	1.38	2.43	0.57	1.38	1.94	2.19
−2.10	1.13	−0.50	1.12	2.31	0.30	1.12	1.67	2.15
−1.81	0.85	−0.79	0.84	2.19	0.01	0.84	1.39	2.09
−1.50	0.55	−1.10	0.54	2.05	−0.30	0.54	1.09	1.98

References

Alhajji, E., Al-Masri, M.S., Khalily, H., Naoum, B.E., Khalil, H.S., Nashawati, A., 2016. A study on sorption of 226Ra on different clay matrices. Bull. Environ. Contam. Toxicol. 97, 255–260.

Altmann, S., 2008. 'Geo'chemical research: a key building block for nuclear waste disposal safety cases. J. Contam. Hydrol. 102, 174–179.

Ames, L.L., McGarrah, J.E., Walker, B.A., 1983. Sorption of trace constituents from aqueous solutions onto secondary minerals. II. Radium. Clays and Clay Minerals 31, 335–342.

Andra, 2001. Référentiel géologique du site de Meuse/Haute Marne. Rapp. A RP ADS 99-005 de l'Agence nationale pour la gestion des déchets radioactifs. Châtenay-Malabry, France.

Baeyens, B., Bradbury, M.H., 2004. Cation exchange capacity measurements on illite using the sodium and cesium isotope dilution technique: effects of the index cation, electrolyte concentration and competition: modeling. Clay Clay Miner. 52, 421–431.

Baeyens, B., Marques Fernandes, M., 2018. 5 - adsorption of heavy metals including radionuclides. In: Schoonheydt, R., Johnston, C.T., Bergaya, F. (Eds.), Developments in Clay Science. Elsevier, pp. 125–172.

Bradbury, M.H., Baeyens, B., 1997. A mechanistic description of Ni and Zn sorption on Na-montmorillonite Part II: modelling. J. Contam. Hydrol. 27, 223–248.

Bradbury, M.H., Baeyens, B., 2009. Sorption modelling on illite Part I: titration measurements and the sorption of Ni, Co, Eu and Sn. Geochem. Cosmochim. Acta 73, 990–1003.

Brouwer, E., Baeyens, B., Maes, A., Cremers, A., 1983. Cesium and rubidium ion equilibriums in illite clay. J. Phys. Chem. 87, 1213–1219.

Curti, E., Fujiwara, K., Iijima, K., Tits, J., Cuesta, C., Kitamura, A., Glaus, M.A., Müller, W., 2010. Radium uptake during barite recrystallization at 23±2°C as a function of solution composition: an experimental 133Ba and 226Ra tracer study. Geochem. Cosmochim. Acta 74, 3553–3570.

Davies, C.W., 1962. Ion Association. Butterworths, Washington.

Ferreira, C.M.H., Pinto, I.S.S., Soares, E.V., Soares, H.M.V.M., 2015. (Un)suitability of the use of pH buffers in biological, biochemical and environmental studies and their interaction with metal ions – a review. RSC Adv. 5, 30989–31003.

Fisher, R.S., 1998. Geologic and geochemical controls on naturally occurring radioactive materials (NORM) in produced water from oil, gas, and geothermal operations. Environ. Geosci. 5, 139–150.

Gaines, G.L.J., Thomas, H.C., 1953. Adsorption studies on clay minerals. II. A formulation of the thermodynamics of exchange adsorption. J. Chem. Phys. 21, 714.

Hidaka, H., Horie, K., Gauthier-Lafaye, F., 2007. Transport and selective uptake of radium into natural clay minerals. Earth Planet Sci. Lett. 264, 167–176.

IAEA, 2014. The Environmental Behaviour of Radium: Revised Edition. INTERNATIONAL ATOMIC ENERGY AGENCY, Vienna.

Károly, L., Zoltán, M., 2012. Claystone as a potential host rock for nuclear waste storage. In: Marta, V., Gražyna Simha, M. (Eds.), Clay Minerals in Nature. IntechOpen, Rijeka. Ch. 4.

Klinkenberg, M., Brandt, F., Baeyens, B., Bosbach, D., Fernandes, M.M., 2021. Adsorption of barium and radium on montmorillonite: a comparative experimental and modelling study. Appl. Geochem. 135, 105117.

Marques Fernandes, M., Baeyens, B., 2019. Cation exchange and surface complexation of lead on montmorillonite and illite including competitive adsorption effects. Appl. Geochem. 100, 190–202.

Marques Fernandes, M., Klinkenberg, M., Baeyens, B., Brandt, F., 2023. Experimental Data for: Adsorption of Ba and 226Ra on Illite: a Comparative Experimental and Modelling Study, V2 ed. Jülich DATA.

Martin, A.J., Crusius, J., Jay McNee, J., Yanful, E.K., 2003. The mobility of radium-226 and trace metals in pre-oxidized subaqueous uranium mill tailings. Appl. Geochem. 18, 1095–1110.

Missana, T., Colàs, E., Grandia, F., Olmeda, J., Mingarro, M., García-Gutiérrez, M., Munier, I., Robinet, J.-C., Grivé, M., 2017. Sorption of radium onto early cretaceous clays (Gault and Plicatules Fm). Implications for a repository of low-level, long-lived radioactive waste. Appl. Geochem. 86, 36–48.

Montoya, V., Baeyens, B., Glaus, M.A., Kupcik, T., Marques Fernandes, M., Van Laer, L., Bruggeman, C., Maes, N., Schäfer, T., 2018. Sorption of Sr, Co and Zn on illite: batch experiments and modelling including Co in-diffusion measurements on compacted samples. Geochem. Cosmochim. Acta 223, 1–20.

Nagra, 2002. Project Opalinus Clay: Safety Report. Demonstration of Disposal Feasibility (Entsorgungsnachweis) for Spent Fuel, Vitrified High-Level Waste and Long-Lived Intermediate-Level Waste. Nagra, Wettingen, Switzerland. Nagra Technical Report NTB 02-05.

Nagra, 2014. Miram 14 – model inventory for radioactive materials. In: National Cooperative for the Disposal of Radioactive Waste, p. 108. Switzerland.

Ondraf, 2001. SAFIR 2: Safety Assessment and Feasibility Interim Report 2. NIROND-2001-06 E. Ondraf. Brussels, Belgium.

Perrin, Dempsey, 1974. In: Hall, C.a. (Ed.), Buffers for pH and Metal Ion Control. London.

Poinssot, C., Baeyens, B., Bradbury, M.H., 1999. Experimental and modelling studies of caesium sorption on illite. Geochem. Cosmochim. Acta 63, 3217–3227.

Robin, V., Tertre, E., Beaucaire, C., Regnault, O., Descostes, M., 2017. Experimental data and assessment of predictive modeling for radium ion-exchange on beidellite, a swelling clay mineral with a tetrahedral charge. Appl. Geochem. 85, 1–9.

Tachi, Y., Shibutani, T., Sato, H., Yui, M., 2001. Experimental and modeling studies on sorption and diffusion of radium in bentonite. J. Contam. Hydrol. 2–4, 171–186.

Tertre, E., Prêt, D., Ferrage, E., 2011. Influence of the ionic strength and solid/solution ratio on Ca(II)-for-Na+ exchange on montmorillonite. Part 1: chemical measurements, thermodynamic modeling and potential implications for trace elements geochemistry. J. Colloid Interface Sci. 353, 248–256.

Wagner, J.F., 2013. Chapter 5.3 - clay liners and waste disposal. In: Bergaya, F., Lagaly, G. (Eds.), Developments in Clay Science. Elsevier, pp. 663–676.

Westall, J., Zachary, J.L., Morel, F., 1976. MINEQL, a Computer Program for the Calculation of Chemical Equilibrium Composition of Aquous Systems. Technical Note 18. Department of Civil Engeneer, Massachusetts Institute of Technology, Cambridge, Massachusetts.

Xu, Y., Liang, X., Xu, Y., Qin, X., Huang, Q., Wang, L., Sun, Y., 2017. Remediation of heavy metal-polluted agricultural soils using clay minerals: a review. Pedosphere 27, 193–204.

Yuan, G.D., Theng, B.K.G., Churchman, G.J., Gates, W.P., 2013. Chapter 5.1 - clays and clay minerals for pollution control. In: Bergaya, F., Lagaly, G. (Eds.), Developments in Clay Science. Elsevier, pp. 587–644.

Zhang, P.-C., Brady, P.V., Arthur, S.E., Zhou, W.-Q., Sawyer, D., Hesterberg, D.A., 2001. Adsorption of barium(II) on montmorillonite: an EXAFS study. Colloids Surf. A Physicochem. Eng. Asp. 190, 239–249.

Zhu, R., Chen, Q., Zhou, Q., Xi, Y., Zhu, J., He, H., 2016. Adsorbents based on montmorillonite for contaminant removal from water: a review. Appl. Clay Sci. 123, 239–258.